Volume 4 MAY, 1933 Number 5

PHYSICS

A Journal of General and Applied Physics

An X-Ray Study of Variations in the Structure of Wood Fiber Walls*

CHARLES W. STILLWELL, *Department of Chemistry, University of Illinois*

(Received March 7, 1933)

Characteristic x-ray diffraction patterns produced by transverse, radial and tangential sections of wood fibers have been discussed. There are two fundamental types of orientation of the micelles or fibrils in wood fibers: A, parallel to the fiber axis; B, parallel to each other, but on a spiral at a definite slope to the fiber axis. The deviation from either type may be qualitatively estimated from the diffraction pattern. For type B, the slope of the spiral may be measured with considerable accuracy. When large angles of slope of the micelles are indicated most wood fibers differ fundamentally from cotton. In wood fibers the average slope is at a definite angle to the fiber axis; the deviation is from Type B. In cotton fibers the average slope approaches 0°; the deviation is from Type A.

IT has been understood for some time that the cell walls of plants in general are built up from groups of micelles, these groups being arranged in a more or less regular fashion, either parallel to the fiber axis or spirally around the cell wall, sometimes at a fairly definite angle to the fiber axis.[1]

Concerning the wood fiber in particular there is indirect evidence that the micelles[2] are laid down spirally in the wall. The microscopic checks, in compression wood,[3] which are always at a fairly constant angle to the fiber axis in a given fiber, suggest this. Frey, Koehler[4] and others, using polarized light have measured the angle of slope of the crystalline groups in the cell wall by determining the position of greatest refractive index. They find that this slope often corresponds with that of the fine checks in the wall. Fig. 1 shows a highly magnified model of

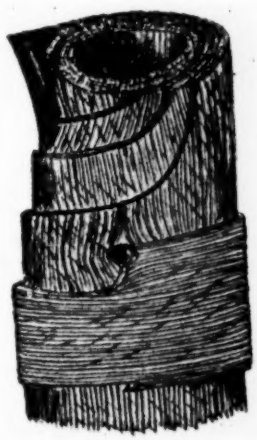

FIG. 1. Model of coniferous wood fiber according to G. W. Scarth.

* The work reported in this paper has been carried on in cooperation with the Forest Products Laboratory, Madison, Wisconsin. The author is indebted to the laboratory for all the specimens of wood used and for many helpful criticisms of the discussion.

[1] D. B. Anderson, Ohio J. Sci. **28**, 299 (1928), gives a general discussion of all the data—microscopic, polarized light and x-ray—pertaining to cell-wall structure.

[2] The micelle is understood to bear the following relation to other recognized structural units in wood: The unit cells of crystalline cellulose joined end to end form cellulose chains. Bundles of parallel chains, about 60A thick and 500–1000A long are said to form micelles. Groups of micelles form fusiform bodies which in turn are supposed to form fibrils. The fibrils make up the wall.

[3] Wood which is formed on the under side of boughs and of leaning trunks of coniferous trees.

[4] Frey, Naturwiss. **15**, 760 (1927). Koehler, Private Communications.

a fiber of a coniferous wood designed by Scarth[5] from microscopic data. Freudenberg has described the structure of the individual micelle and one common orientation of these micelles in wood fibers.[6]

Characteristic x-ray patterns of wood have been published by several authors. Pienkowski[7] and Schmidt[8] have studied systematically certain variations in the structure of wood fiber walls, by means of x-ray patterns produced when an x-ray beam is passed through a tangential section.

In the course of an extended investigation of variations in wood fiber walls and the influence of conditions of growth on the structure of the wood fiber, involving the collection of several hundred diffraction patterns,[9] we have found that one of the most common types of orientation in wood fiber walls has not been described heretofore by x-ray investigation, although it is implied by the microscopic evidence.

Interpretation of Diffraction Patterns

Patterns from transverse sections

When the x-ray beam is passed parallel to the long axes of the wood fibers the pattern usually shows only Debye rings indicating that there is no preferred orientation of the cellulose micelles. Sponsler[10] has suggested that they may be oriented in the fiber wall with the same planes always facing the lumen. They would then be in random array with respect to the x-ray beam.

Occasionally there are intensity maxima on the rings of the pattern from a transverse section. These may be produced by micelles oriented in the rays. Under these conditions there would be a difference between the diffraction patterns of tangential and radial sections. They may also be due to the orientation of the cellulose in the primary layer of the wood fibers themselves. Many wood fibers are flattened to give a nearly rectangular cross section. In such cells the primary layer composed of fibrils sloped at almost 90° to the fiber axis (see Fig. 1) shows activity under polarized light. Micelles so oriented would produce the intensity maxima observed. The study of diffraction by transverse sections of wood is being continued.

Patterns from tangential sections of wood

In general, radial and tangential sections produce similar patterns.

The two types of patterns usually associated with wood fibers are shown diagrammatically. The pattern in Fig. 2a is produced by fibers in which the micelles or fibrils are oriented parallel to the long axis of the cell. The orientation which would produce this pattern is indicated in Fig. 2b. When the orientation varies somewhat from the parallel arrangement so that the fibrils lie on spirals, the pattern of Fig. 3 is produced. The variation in the slope of the fibrils may be estimated by measuring the angle subtended by the more intense arcs.

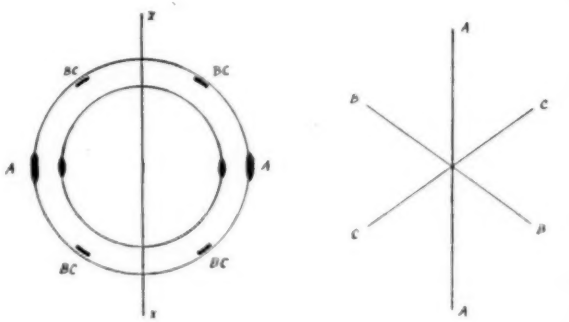

Fig. 2. (a) Diagram of diffraction pattern. Maple, tangential section. Cellulose micelles in cell wall well oriented nearly parallel to fiber axis. X = fiber axis. (b) A–A is the longitudinal axis of wood fibers; the long axis of cellulose crystals and micelles; and the crystal planes which produce maxima A in Fig. 2a. B–B and C–C are the crystal planes which produce maxima B in Fig. 2a.

The diffraction pattern which has not been emphasized in earlier work is shown in Fig. 4a.[11] It is commonly produced by the "compression wood" of conifers. The pattern is characterized by the appearance of four intensity "point"

[5] Scarth, Trans. Roy. Soc. Canada, Section V, [3] **23**, 263 (1929).

[6] K. Freudenberg, J. Chem. Education **9**, 1171 (1932).

[7] S. Pienkowski, Zeits. f. Physik **63**, 610 (1930).

[8] B. Schmidt, Zeits. f. Physik **71**, 696 (1931).

[9] Cu K radiation from a Mueller tube; 45 minutes to 2 hours exposure at 35 kv and 30 m.a.; thickness of specimen one millimeter or less.

[10] Sponsler, Ind. Eng. Chem. **20**, 1060 (1928).

[11] Clark, Sisson and Ritter (Ind. Eng. Chem. **22**, 474 (1930)) published one pattern of this type but it was considered as an exceptional case and no serious attempt was made to interpret it.

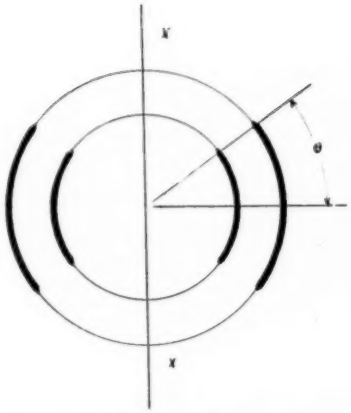

FIG. 3. Diagram of diffraction pattern. Redwood, tangential section. Cellulose micelles imperfectly oriented. The angle θ is a measure of deviation from parallel orientation of Fig. 2a.

maxima *A* rather than the two arcs as in Fig. 3. The same pattern has been produced as follows: A section of maple (the same specimen which produces the pattern of Fig. 2a) was mounted on a goniometer in a cylindrical camera and set with the longitudinal axis of the fibers inclined at $\theta°$ to the axis of rotation. The specimen was then rotated through 360° during the exposure. It is evident, both from the appearance of the pattern and from this rotation experiment that Fig. 4a is produced by fibrils which are oriented parallel to each other and lying on a spiral, sloped at an angle θ to the longitudinal axis of the wood fiber, as shown in Fig. 4b.

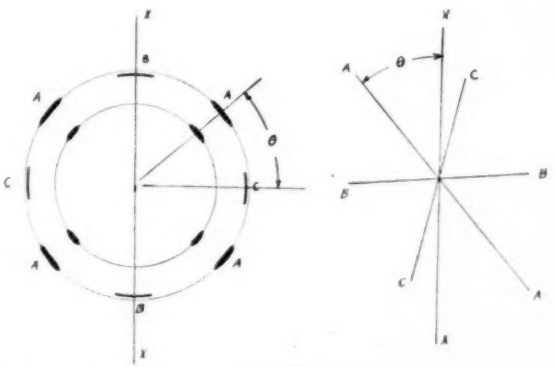

FIG. 4. (a) Diagram of diffraction pattern. Redwood, tangential section. Cellulose micelles oriented parallel to each other, but spirally in the cell wall sloped at angle θ to the fiber axis. X = fiber axis. (b) Position of planes in celulose crystals which produce Fig. 2a when rotated about the axis X. A–A is the long axis of micelles and cellulose crystals; planes which produce maxima A in Fig. 4a. B–B are the planes which produce maxima B in Fig. 4a. C–C are the planes which produce maxima C in Fig. 4a. θ is the angle of slope of micelles in cell wall.

In addition to the four principal intensity maxima (*A* in Fig. 4a), the two maxima (*B* in Fig. 4a) are usually evident. These are produced by the cellulose crystal planes in position *B* (shown in Fig. 4b), the same planes which produce the maxima *B* in Fig. 2a. If the angle θ approaches 45° there are eight intensity maxima clearly visible as indicated (*A*, *B*, *C* in Fig. 4a). The maxima *C* are produced by the planes *C* (Fig. 4b), the same which produce the maxima *C* in Fig. 2a. Wood patterns which show six maxima ($A+B$) appear elliptical since the maxima *B* lie nearer the center of the pattern than those at *A*. Patterns showing all eight maxima appear circular since *B* and *C* correspond to the same interplanar spacing and both lie nearer the center than *A*.

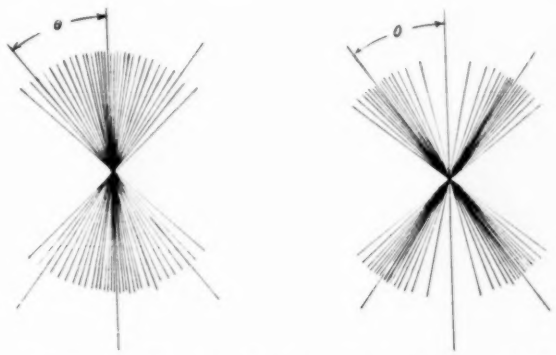

FIG. 5. (a) Diagram showing distribution of micelles deviating from parallel orientation of Fig. 2b. This orientation produces Fig. 3 and is characteristic of cotton. (b) Diagram showing distribution of micelles deviating from spiral orientation of Fig. 4b. This orientation produces a pattern similar to Fig. 4a in which maxima *A* are diffused along the Debye rings.

It is important to emphasize the distinction between the orientations indicated by Figs. 3 and 4a, a distinction which is not always made clear in describing cellulose fibers.

Fig. 3 is produced by fibrils which deviate from an orientation parallel to the fiber axis, and lie on spirals *at various slopes* to the fiber axis. When the angle θ is measured the deviation from the parallel orientation is measured (see Fig. 5a). Fig. 4a, on the other hand, is produced by fibrils which are well oriented parallel to each other, but lie on a spiral *at a constant slope* (θ) to the fiber axis. The orientation which produces Fig. 4a is just as perfect as that producing Fig. 2a.

In examining the actual diffraction patterns, the distinction between types III and IV is not always easy to make. If intensity maxima, even though not well developed, can be detected in the positions *A* (of Fig. 4a) it indicates that the slope of the fibrils deviates from the constant spiral slope of Fig. 4 (as shown in Fig. 5b). This departure from perfect orientation might occur in at least four ways. First, when the fibers themselves are not straight and parallel. This factor has been partially eliminated by using straight grained specimens although the fibers always tend to bend around the rays. Second, when the slope of the spiral in the fiber wall is not constant for all the fibers through which the x-ray beam passes. Third, when the micelles in the spiral in a single fiber wall are not parallel to each other. Fourth, when as suggested by Scarth,[5] the slope is not constant in successive layers of the same fiber wall. It is impossible and probably not essential to choose between the last three by the method used. Microscopic measurements[12] of the angle of slope of the spiral in a group of one hundred tracheids in redwood normal springwood (which produces diffuse intensity maxima *A* in Fig. 4a) showed a wider variation than measurements for one hundred tracheids of redwood compressionwood summerwood (which produces sharp intensity maxima, *A* in 4a). Diffraction patterns for the actual specimens on which these measurements were made are reproduced in Figs. 6 and 7. It is possible, therefore, to estimate qualitatively from the diffuseness of these maxima the degree of deviation from a constant slope. The angle of slope may be accurately measured as indicated in the figures.

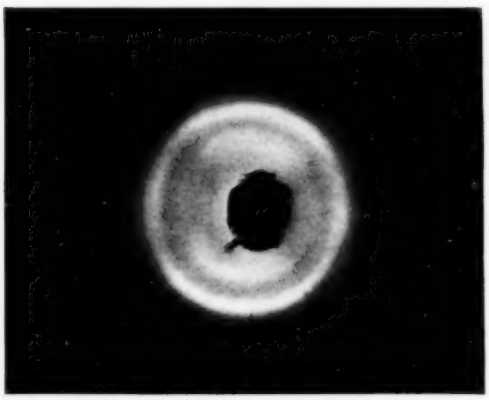

FIG. 6. Actual diffraction pattern. Redwood, tangential section. Normal springwood. Micelles deviate considerably from orientation on spiral. Compare with Fig. 7.

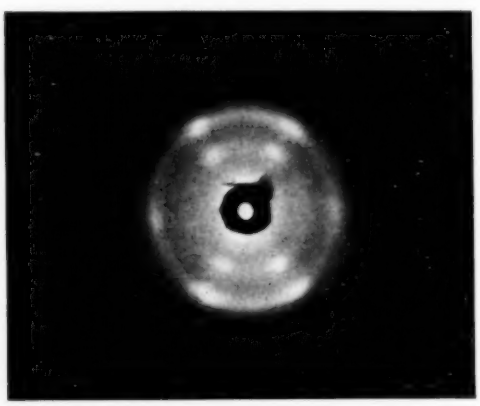

FIG. 7. Actual diffraction pattern. Redwood, tangential section. Compression summerwood. Micelles are well oriented on spiral. Compare with Fig. 6.

GENERAL DISCUSSION

These patterns have an important bearing on the interpretation of x-ray data for cotton and that mentioned above for wood.

Orientation of fibrils in cotton

When an x-ray beam is passed through a bundle of fibers perpendicular to the fiber axis ramie produces a diffraction pattern part of which is shown in Fig. 2a. If this bundle is twisted so that the fiber axes are aligned spirally with respect to the axis of the bundle as a whole, the x-ray beam still perpendicular to the axis a pattern of the general type of Fig. 3 is obtained.[13] The intensity of the arcs is greatest at the equator. Natural cotton fibers produce a similar pattern. This has been accepted as a confirmation of the microscopic evidence[14] that in cotton the cellulose fibrils are arranged spirally in the cell wall. Since the arcs are most intense at the

[12] The author is indebted to Arthur Koehler of the Forest Products Laboratory for these data.

[13] K. Hess, *Die Chemie der Zellulose und Ihrer Begleiter*, p. 647, Leipsic, 1928.

[14] See, among other, W. L. Ball and H. A. Hancock, Proc, Roy. Soc. (London) **B93**, 426 (1923) and Farr and Clark. Contributions of Boyce Thompson Institute **4**, 273 (1932).

equator, the fibrils deviate from the parallel orientation of Fig. 2, and are sloped at various angles to the fiber axis. The pattern produced by twisting a bundle of ramie fibers is not that of fibers oriented on a spiral at a constant angle of slope. The microscopic evidence indicates that in cotton the angle of slope of these spiral fibrils varies through wide limits.[14] In spite of this it is often assumed and has recently been restated that in cotton the micelles are "inclined at a constant angle to the fiber axis,"[15] but this cannot be the case.

Orientation in wood

Pienkowski[7] and Schmidt[8] have obtained x-ray patterns for wood resembling Figs. 2a and 3. From the extent of the arcs from the equator along the Debye rings they estimate the degree of orientation of the cellulose micelles. It is implied that the arcs are caused by a wide deviation of the micelles from the mean direction, the latter being parallel to the axis of the wood cells. They make no suggestion of cellulose micelles oriented spirally in the cell wall at a more or less constant angle. The data on which the present discussion is based, however, indicate that in most wood fiber walls, when the micelles or fibrils are not parallel the deviation is from the orientation of Fig. 4 rather than Fig. 2. This is more in accordance with the microscopic data.

The relation of the structure of wood fibers to species and conditions of growth

Recently it has been found that the slope of the fibrils in wood fiber walls bear an important relation to some of the physical properties of wood (density, longitudinal shrinkage, tensile strength, etc.).[16] It would be desirable, therefore, if some relation could be found between this slope and the species or conditions of growth of woods. Although a preliminary study[11] suggested such a possibility, it is now evident that no sweeping generalizations may be made. There are indications of limited relationships and these will be extended and reported in a later paper.

[15] Astbury, *Annual Reports*, London, 1932, p. 327. The reference in *Annual Reports* is to the work of Herzog and Jancke, Zeits. f. Physik. Chemie **A139**, 235 (1928). In the original paper there appears to be no emphasis of orientation at a constant angle. It is stated that the micelles show spiral orientation.

[16] Beyer, Thesis, University of Wisconsin, 1930. Dice, Thesis, University of Wisconsin, 1931.

The Converse Piezoelectric Effect in Mixed Crystals Isomorphous with Rochelle Salt*

SIDNEY BLOOMENTHAL, *RCA Victor Company, Camden, New Jersey*

(Received March 15, 1933)

The temperature dependence of the piezoelectric strain constant d_{14} was investigated in mixed crystals isomorphous with Rochelle salt. Crystals oriented for utilization of Voigt's theory of the converse piezoelectric effect in the hemihedral class of the orthorhombic system were grown at constant temperature from supersaturated solutions of Rochelle salt containing isomorphous impurities $C_4H_4O_6Na\,NH_4\cdot 4H_2O$ or $C_4H_4O_6Na\,Tl\cdot 4H_2O$ and measurements of the strain resulting from an applied electric field were made in the range 10 to 35°C. Hysteresis and saturation occur in the range of large piezoelectric activity where d_{14} evaluated from the straight portion of the strain curve is approximately 5×10^{-4} in both the pure salt and mixed crystal, a value several times as large as that reported from measurements of the direct effect in Rochelle salt. The critical temperature for a mixed crystal lies below that of pure Rochelle salt (25+273°K) and the shift observed compares favorably in magnitude with the value calculated from the dipole theory of dielectrics. The region in which d_{14} decreases to about 10^{-5} covers 3°C. The value of d_{14} diminishes further as the temperature is raised. d_{14} is defined as twice the change in length per cm length of a narrow crystal cut at 45° with the Y and Z axes when unit electrostatic field is applied in the X direction.

INTRODUCTION

IN order to explain the peculiar behavior of Rochelle salt near 25°C, several experimenters have postulated a critical temperature for this dielectric analogous to the Curie point for ferromagnetic materials.[1] When a ferromagnetic element is alloyed with a second element, the Curie point is shifted.[2] If the viewpoint taken for Rochelle salt is correct, one may expect as further evidence an analogous shift of the critical temperature in mixed crystals grown from Rochelle salt solutions containing isomorphous impurities and reported on in this paper.

The usual method of measuring the piezoelectric constant of Rochelle salt crystals cut at right angles to the X axis is subject to criticism because it does not take into account the conductivity.[3] When one measures the deformation of a piezoelectric crystal resulting from a known applied electric field, he can secure the piezoelectric constant without the difficulty due to conductivity. Hence in this investigation the piezoelectric constant is evaluated from measurements of the converse effect. Because of the well-known relation between the dielectric and piezoelectric constants of a crystal,[4] it is to be expected that any abrupt variation of the dielectric properties with temperature will be paralleled by similar behavior of the piezoelectric properties. The piezoelectric effect is greater in Rochelle salt than in any other known substance. Between the temperatures −20 and +25°C the piezoelectric constant d_{14} is about $25{,}000\times 10^{-8}$, determined from the polarization resulting when pressure is applied to a suitably cut crystal.[5] Near 20°C d_{25} and d_{36}, which show no abrupt variation with temperature, have the values -165×10^{-8} and 35.4×10^{-8}, respectively.[6, 7] Table I deals with the family of tartrates to which Rochelle salt belongs. These tartrates are isomorphous because of the similarity in size of the replaceable ion K^+, Tl^+, Rb^+ or NH_4^+, and value of the axial ratio. A seed of Rochelle salt will grow in a supersaturated solution of any of these salts or mixtures of them. Mandell investigated the direct piezoelectric effect in sodium ammonium tartrate.[8] He found $d_{14}=56\times 10^{-8}$, $d_{25}=-149.5\times 10^{-8}$ and

* Presented at the Cambridge Meeting of the A.P.S. February 25, 1932. See Phys. Rev. **40**, 121A (1932).

[1] J. Valasek, Phys. Rev. **19**, 489 (1922); P. Kobeko and J. Kurtchatov, Zeits. f. Physik **66**, 192 (1930).

[2] P. Weiss and G. Foex, Int. Crit. Tab. **VI**, 406 (1929).

[3] R. D. Schulwas-Sorokin, Phys. Rev. **34**, 1448 (1929).

[4] M. Born, *Atomtheorie des Festen Zustandes*, p. 561, 1923.

[5] R. D. Schulwas-Sorokin, Zeits. f. Physik **73**, 700 (1932).

[6] F. Pockels, Gött. Abh. p. 69, 1893.

[7] J. Valasek, Science **65**, 235 (1927).

[8] W. Mandell, Proc. Roy. Soc. **A121**, 130 (1929).

TABLE I. *Double salts of d-tartaric acid isomorphous with Rochelle salt.*

Substance[1]	K replaced by[2]	Axial ratio	Density
Sodium potassium tartrate $C_4H_4O_6KNa.4H_2O$ (Rochelle salt)[3]		0.8317 : 1 : 0.4296	1.790
Sodium rubidium tartrate $C_4H_4O_6RbNa.4H_2O$	Rb	0.8328 : 1 : 0.4388	—
Sodium ammonium tartrate $C_4H_4O_6NH_4Na.4H_2O$	NH_4	0.8233 : 1 : 0.4200	1.587
Sodium thallium tartrate $C_4H_4O_6TlNa.4H_2O$	Tl	0.8491 : 1 : 0.4307	2.580

[1] Groth in Chemische Krystallographie, Vol. III, p. 315 and 332 lists these in the bisphenoidal class of the rhombic system.

[2] Ionic Radii are for K^{+1}, $r=1.33$A, Rb^{+1} $r=1.49$A, NH_4^{+1} $r=1.43$A and Tl^{+1} $r=1.49$A according to Goldschmidt, Trans. Faraday Soc. **25–26**, 253 (1929).

[3] Also written

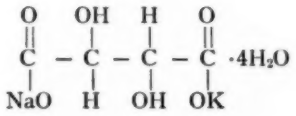

$d_{36}=28.3\times10^{-8}$ with no dependence of these values upon temperature in the range -17 to $+30$°C. By a resonance method similar to that used by Giebe and Scheibe for the qualitative study of the piezoelectric properties of a variety of crystals,[9] the writer found the piezoelectric response from sodium thallium tartrate to be less than that from sodium ammonium tartrate. The piezoelectric properties of sodium rubidium tartrate have not been investigated. Thus far we know that Rochelle salt is the only member of the series of pure isomorphous tartrates described in Table I that has a large piezoelectric constant near room temperature. This paper deals with the large piezoelectric constant of mixed crystals, sodium potassium tartrate—sodium ammonium tartrate and sodium potassium tartrate—sodium thallium tartrate. The shift in the critical temperature with change of the crystal's composition can be computed if one makes use of the Debye dipole theory of dielectrics.[10]

[9] E. Giebe and A. Scheibe, Zeits. f. Physik **33**, 760 (1925).

[10] P. Debye, *Theorie der elektrischen und magnetischen Molekulareigenschaften*, Marx, Handbuch der Radiologie **VI**, 597 (1924).

GROWTH OF THE PIEZOELECTRIC CRYSTALS AND MEASUREMENT OF THEIR CONVERSE PIEZOELECTRIC PROPERTIES

The method of crystal growing used in this work employs seeds oriented for utilization of Voigt's equations for the converse piezoelectric effect in Rochelle salt.[11] These are the following:

$$y_z=d_{14}E_x=\Delta l_1/l_1\beta\gamma,$$
$$z_x=d_{25}E_y=\Delta l_2/l_2\gamma\alpha, \qquad (1)$$
$$x_y=d_{36}E_z=\Delta l_3/l_3\alpha\beta.$$

y_z, z_x, x_y are shearing strains in the YZ, ZX, XY planes respectively, d_{14}, d_{25}, d_{36} are the piezoelectric strain constants. (Cady's change of Voigt's terminology.[12]) E_x, E_y, E_z are the electric field strengths in the X, Y or Z directions. l_1, l_2, l_3 are lengths of crystal making angles with the Y and Z, Z and X, X and Y axes, having cosines β and γ, γ and α, α and β. Δl_1, Δl_2, Δl_3 are small changes in l_1, l_2, l_3. For the maximum effect

$$\alpha=\beta=\gamma=1/2^{\frac{1}{2}}, \qquad (2)$$

$$\Delta l_1/l_1=d_{14}Vx/600x, \quad \Delta l_2/l_2=d_{25}V_y/600y, \quad \Delta l_3/l_3=d_{36}V_z/600z, \qquad (3)$$

where V_x, V_y, V_z are the potential differences in volts applied across the x, y or z crystal thicknesses in cm. Fig. 1 illustrates the linear effect

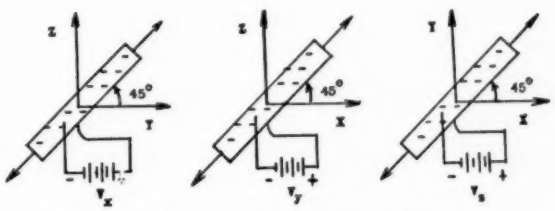

FIG. 1. Relation between linear deformation and direction of applied electric field for narrow crystals of Rochelle salt having foiled faces and cut at 45° with the principal axes shown.

and takes into account the signs of the measured constants. The system of axes chosen is a right-handed one. The strain becomes a contraction

[11] W. Voigt, *Die Fundamentalen Physikalischen Eigenschaften der Krystalle*, pp. 123, 203, 1898; *Lehrbuch der Krystallphysik*, p. 873, 1910.

[12] W. G. Cady, Proc. I.R.E. **18**, 2136 (1930).

when the sign of the applied field is changed. The final Eqs. (3) are directly applicable to measurement of the strain in suitably cut slabs of crystal when the electric field is applied, and the piezoelectric constants can be deduced. The dimensions of d_{14}, etc., are $l^{\frac{1}{2}}\epsilon^{\frac{1}{2}}m^{-\frac{1}{2}}t$ and check with those given by the equations for the direct effect.[13]

In order to reduce the time required for growth and preparation of crystals for measurement, a method of growing crystals oriented for utilization of Eqs. (3) was adopted. Moore and Christopher of the General Electric Company originated this method of growing piezoelectric crystals.[14] For example: to grow a crystal which will shear in the YZ plane when an electric field is applied in the X direction, one cuts a seed with faces (form 100) perpendicular to the X axis (X cut) and places it between parallel rust-proofed metal or glass plates, separated by spacers whose thickness determines the x value of the final rectangular plate of crystal. From seeds cut out of several such plates presented to the writer by Dr. Moore, a strain of piezoelectric Rochelle salt crystals was propagated.

Fig. 2 illustrates the development of planes for each of the three types of piezoelectric

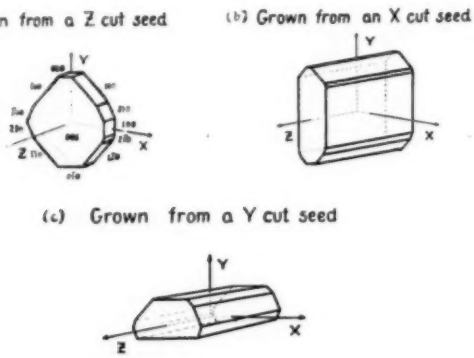

FIG. 2. Oriented piezoelectric Rochelle salt crystals.

crystal. The one grown from the Z cut seed utilizes the d_{36} shearing constant, the one from the X cut seed the d_{14} constant, and the lower one, grown from a Y cut seed, used the d_{25} constant when an electric field is applied across the thickness of the plate. The zone with $Z=\infty$ is prominent, but not all the members present in the crystal grown from the Z cut seed are present in the other two.

Two improvements were made upon the method of Moore and Christopher that deserve mention here.

(1) Spurious or "weed" crystal growth was completely eliminated through the use of tanks sealed air-tight during the growing period and heated at the base to produce circulation with consequent temperature equalization of the mother liquor.

(2) The crystals were grown at constant temperature from aqueous solutions having a known low degree of supersaturation. All of the mixed crystals were grown from X cut seeds of Rochelle salt, since the constant d_{14} is the only one of the three that shows the unusually large temperature coefficient in the pure substance.[7]

To a solution containing a known amount of Rochelle salt, the solution containing the impurity (sodium ammonium or sodium thallium tartrate) was added. In the case of mixed crystals containing sodium ammonium tartrate, the percentage in the crystal was taken equal to the percentage of salt impurity in the growing solution.[15] With sodium thallium tartrate as the impurity, precipitation with potassium iodide of the extremely insoluble thallium iodide from the mixed crystal made possible a quantitative determination of the crystal's composition.

A longitudinal strain at 45° with the Y and Z axes when an electric field is applied in the X direction gives one a convenient displacement for measurement of the d_{14} constant. Fig. 3 shows the combination mechanical and optical lever used to measure this strain. It was constructed under the supervision of Mr. C. C. Rice, working in the laboratories of the Radio Corporation during the summer of 1930, and used by him in a preliminary study of the converse piezoelectric effect in Rochelle salt. An average sized crystal used was 3 cm long, 8 mm wide and 1 mm thick. It was cut from a plate with a sharp scalpel and polished on ground glass. Electrodes of 1 mil thick tinfoil,

[13] N. E. Dorsey, Int. Crit. Tab. I, 29 (1926).

[14] U. S. Patent No. 1,746,144 (February 4, 1930); R. W. Moore, J. Am. Chem. Soc. **41**, 1060 (1919). (Growth of fully developed crystals.)

[15] A. Lavenir, Bull. Soc. Fr. Min. **17**, 153 (1894).

attached with balsam dissolved in xylol, covered all except the lower portion of the faces which were under the supporting clamp. The lever was enclosed in a Thyratron controlled thermostat having a suitable window. The magnification attained is given by $2Aa_2/a_1a_3$ and was 20,400.

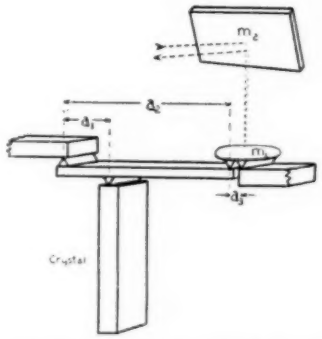

FIG. 3. Mechanical and optical arrangements for measurement of the converse piezoelectric effect.

Here A is the length of optical path from the mirror m_1 to the telescope and scale. d_{14} above 25°C, d_{25} and d_{36} measured for Rochelle salt with this apparatus agreed with the values given by Valasek from measurements of the direct effect. Fig. 4 shows some of the values of

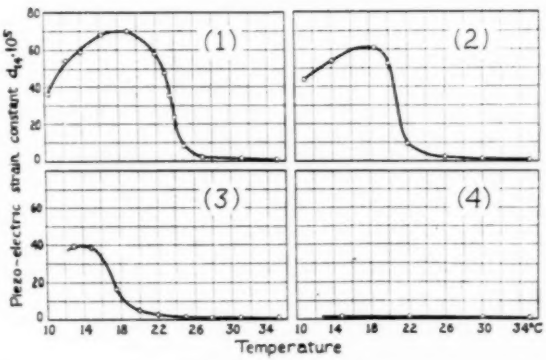

FIG. 4. Variation of the piezoelectric strain constant d_{14} with temperature for a c.p. Rochelle salt crystal (1) and for mixed Rochelle salt crystals with 0.37 percent $C_4H_4O_6Tl\,Na\cdot4H_2O$ (2), 1.0 percent $C_4H_4O_6NH_4\,Na\cdot4H_2O$ (3) and 3.7 percent $C_4H_4O_6Tl\,Na\cdot4H_2O$ (4).

d_{14} measured at different temperatures from the slope of the curves of strain for different field strengths. Saturation, hysteresis and a time lag were present when large value of d_{14} existed below the critical temperature and a complete loop of strain plotted against field strength permitted evaluation of d_{14} if the straight portion of the curve intercepting the strain ordinate was chosen. Somewhat above the critical temperature the relation between strain and electric field strength appears to be a linear one. An investigation with apparatus of ten times the sensitivity used here ought to settle this point definitely for the crystals considered.

The results for the mixed crystal, whose d_{14} variation with temperature is plotted in Fig. 4 (2), are given in Fig. 5 for 14°C and 35°C in

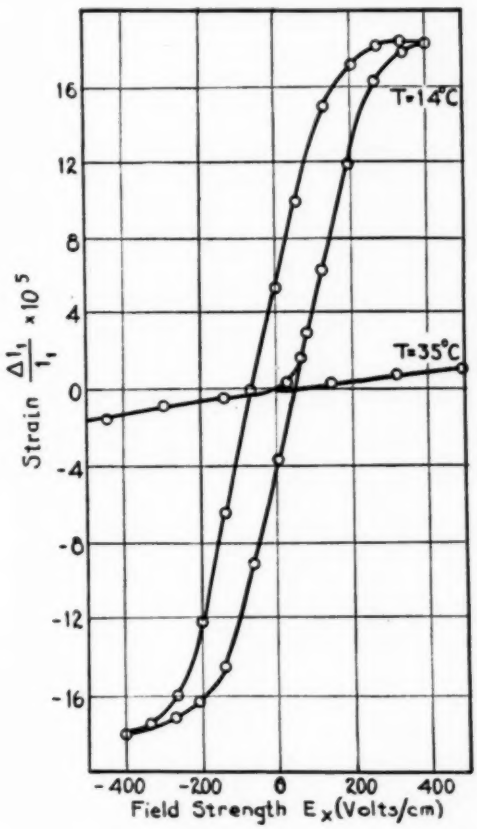

FIG. 5. Converse piezoelectric effect in a mixed Rochelle salt crystal having 0.37 percent $C_4H_4O_6Tl\,Na\cdot4H_2O$ below and above the critical temperature.

order for us to illustrate the type of strain curve secured below and above the critical temperature. Starting with the crystal electrodes at zero potential one gradually increases the voltage supplied from a 3000 ohm potential divider connected across a 67.5 volt heavy duty "B" battery. The applied potential is read on a high-resistance voltmeter at intervals of 10 volts

when the scale reading is taken. Fifteen seconds were given for the scale to come to a steady value before each reading was taken. The voltage was reduced in similar steps after sixty volts was reached, and the left upper portion of the loop in Fig. 5 for $T=14°C$ was secured. For zero potential applied to the crystal a residual strain remains. The potential difference applied was reversed in sign and the lower half of the loop was secured, with observations extended upon a second reversal of the field until the loop closed. d_{14} was evaluated for this case from the slope of the straight portion of the loop. Above the critical temperature Voigt's law is obeyed and d_{14} does not depend upon the field strength in the range investigated. A detailed discussion of the strain curves secured below the critical temperature ought to deal with second order effects due to the polarization of the dielectric by strain in a sense opposite to the applied field, but will not be given at this time. The possibility of plastic deformation ought to be considered also. According to Eq. (3) above, d_{14} is equal to twice the change in length per cm length of the crystal per unit applied electrostatic field.

The Critical Temperature

In order to study the effect of isomorphous impurities upon the piezoelectric properties of Rochelle salt, it is necessary for us to make use of the Debye theory of dielectrics,[10] taking into account the effect of a strong molecular field created by dipoles existing within the crystal. By analogy with the law of Weiss, we have for the susceptibility above the critical temperature Θ,

$$x_1=d/(T-\Theta),$$

where d is a constant and T is the absolute temperature.

$$\Theta=\mu^2\rho n\nu/3k, \tag{4}$$

where μ is the dipole moment, ρ the density of the crystal, n the number of dipoles per gram, ν the molecular field constant and k the Boltzmann constant.

Below the critical temperature the dielectric properties of Rochelle salt are analogous to ferromagnetic properties.

For a crystal having metallic coatings and not piezoelectric

$$D=E_x+4\pi Q, \quad Q=XE_x, \quad D=\delta E_x, \tag{5}$$

Q is the electric moment per cc, D the dielectric displacement and δ the dielectric constant. For the piezoelectric crystals studied

$$y_z=d_{14}E_x, \tag{6}$$

and the back polarization is $e_{14}y_z$. Here e_{14} is the piezoelectric modulus. Modifying (5) above, we have

$$Q_1=XE_x+e_{14}d_{14}E_x. \tag{7}$$

Then

$$X_1=X+e_{14}d_{14}, \tag{8}$$

Q_1 is the electric moment and X_1 the susceptibility of the piezoelectric material, X is the ordinary susceptibility. From Eq. (8) it is clear that at the critical temperature, where the susceptibility becomes extremely large, unusual values of e_{14} and d_{14} will also result.

Let Eq. (4) apply to pure Rochelle salt. The number of dipoles per gram is

$$n=AN/M. \tag{9}$$

Here A is a constant, N Avogadro's number, and M the molecular weight.

For the mixed crystal:

$$\Theta_m=\mu^2\rho_m n_m P\nu/3k. \tag{10}$$

In Eq. (10) P is the fraction of Rochelle salt molecules out of the total number in the mixed crystal and is multiplied by ν to give the molecular field constant for the mixture. The number of dipoles per gram in the mixed crystal is n_m and is equal to AN/M_m with M_m the molecular weight of the mixed crystal. Dividing (10) by (4), one secures after substituting M/M_m for n_m/n

$$\Theta_m=\rho_m MP\Theta/\rho M_m. \tag{11}$$

In the present work percentage by weight was the quantity determined. We wish now to compute P. If a grams of the mixed crystal have p_1 percent of impurity of molecular weight M_1 and $100-p_1$ or p_2 percent of Rochelle salt,

$p_2Na/100M$ = number of Rochelle salt molecules in a grams.

$p_1Na/100M_1$ = number of molecules of isomorphous impurity in a grams.

$$P = p_2/(p_2 + Mp_1/M_1). \quad (12)$$

When small quantities of impurity only are considered, ρ_m and M_m will not differ appreciably from ρ and M. Thus

$$\Theta_m = P\Theta, \quad (13)$$

and the shift in the critical temperature is

$$\Delta\Theta = \Theta - \Theta_m = (1-P)\Theta. \quad (14)$$

Table II gives a comparison between a few values of $\Delta\Theta$ estimated from the observed variation of d_{14} with temperature and those calculated from Eq. (14). For pure Rochelle salt $\Theta = 25 + 273°K$ where d_{14} is 8400×10^{-8}. The value of temperature for which d_{14} had a similar value in the case of the mixed crystals was taken as Θ_m. In Table II, a refers to sodium ammonium tartrate as the impurity, and b to sodium thallium tartrate. The observed shift in every case is larger than the calculated value. In view of the fact that the rapid change in d_{14} extends over about 3°C the limit of error is large in the determination of $\Delta\Theta$ and only a qualitative agreement with the theory can be expected.

TABLE II. *Comparison between observed and calculated values of* $\Delta\Theta$.

Isomorphous impurity	P	Θ_m	$\Delta\Theta$ Observed	$\Delta\Theta$ Calculated	Shown in curve
b	0.9977	22.5+273°K	2.5°C	0.686°K	(2) Fig. 4.
a	.9973	22.0+273°K	3.0	0.806	Not shown
a	.9892	19.0+273°K	6.0	3.220	(3) Fig. 4.
b	.9767	—	—	6.961	(4) Fig. 4.

In a paper entitled *Über Die Elektrischen Eigenschaften der Seignettesalz-Mischkristalle*, Kurtschatow and Eremejew[16] reported on the dielectric properties of a mixed crystal containing 100 molecules of Rochelle salt for every 140 molecules of a salt in which potassium is replaced by ammonium. The range of unusual electrical activity extended from −107°C to the temperature of liquid air. Referring to Eq. (11) above we see that Θ_m is 132°K for the case where P equals 100/240 and ρ_m and M_m lie between the values known for pure sodium ammonium and sodium potassium tartrates, a value somewhat lower than that found by the Russian observers.

[16] B. Kurtschatow and M. Eremejew, Phys. Zeits. d. Sow. **1**, 1 (1932).

Operating Constants for Direct-Current Thermionic Amplifiers

P. A. MACDONALD AND T. W. TWEED, *Department of Physics, University of Manitoba, Canada*

(Received March 6, 1933)

The sensitivity to voltage, measured in volts per mm scale deflection, of a direct-current thermionic amplifier (simple circuit) is taken as inversely proportional to the mutual conductance divided by the plate current of the valve employed. The mutual conductance is found to decrease less rapidly than the plate current, as the filament and plate potentials are lowered. The most sensitive operating value of the plate potential of a UX 222 is found to be 1.5 volts giving a voltage sensitivity of 8×10^{-4} volt/mm in the simple circuit with no plate current compensation. By suitable use of the screen grid, a grid-filament resistance of 10^{14} ohms may be obtained giving a current sensitivity of 8×10^{-15} amp./mm with an input resistor of 10^{11} ohms.

THE output of a thermionic amplifier is obtained from the plate circuit in which a steady plate current is always flowing. With the amplification of alternating currents the plate circuit may be considered as containing the steady direct plate current with a superimposed alternating current, which may be readily separated by a transformer or condenser coupling. Where direct currents are being amplified, however, both the amplified and plate currents are continuous and flowing in the same circuit and their separation constitutes a difficult problem.

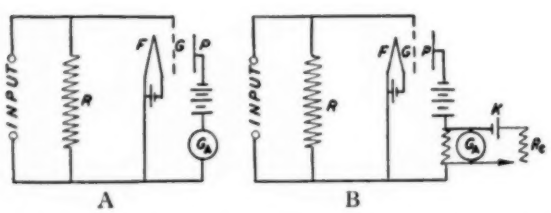

FIG. 1. These two circuits demonstrate the basic principles of all direct-current amplifiers.

The simple circuit of Fig. 1A constitutes the basis of practically all direct-current amplifiers. In this circuit the steady plate current flows through the circuit *PGF* causing a deflection of the galvanometer *Ga*. Forcing a current through the input resistance *R* with an external e.m.f. raises the potential of *G* relative to *F* causing an increase in the plate current and a correspondingly greater deflection of the galvanometer. It will be apparent that in order to use a circuit of this type the increment of the galvanometer deflection caused by the current through the grid resistor must be sufficiently great to be perceptible. That is, the amplified current must approximate the same order of magnitude as the plate current, hence the smaller the plate current the more sensitive the amplifier, all other factors being constant.

The usual method of reducing the plate current flowing through the galvanometer is to hold all other factors constant and apply a back e.m.f. to this instrument from an auxiliary source. Fig. 1B shows a circuit exhibiting in its simplest form this principle. The auxiliary battery *K* causes a current, the magnitude of which is controlled by the resistance R_c, to flow through the galvanometer in the opposite direction to the plate current, which is thus balanced out of the circuit allowing the galvanometer to record only the amplified current. This instrument may then be increased in senstivity a limit being placed only by the degree of exactitude and constancy of the balance. Maximum sensitivity is obtained by this method when the balance is made with the plate current from a second vacuum tube, the characteristics of which have been adjusted to match those of the amplifying tube, so that fluctuations in the operating potentials are compensated in the plate circuit.

In examining the work of investigators with direct currents, one is struck with the fact that in practically all cases the operating constants used with valves are those recommended by the manufacturers for alternating-current work.

In this field, since the relative magnitudes of the plate and amplified currents are of no particular importance one would use as large operating potentials as possible in order to obtain the maximum output. From what has been said of direct currents, however, it will be apparent that the controlling factor for voltage sensitivity with this type of amplification is the magnitude of the plate current, which should be as small as possible.

Another point of difference between alternating and direct-current amplification is that with direct currents the limit of the input resistor that may be employed depends only upon the natural resistance existing between the grid and filament. This factor has been thoroughly examined by a number of investigators,[1, 2, 3, 4] and will be referred to in greater detail later.

It is the purpose of this communication to show that there exist operating constants which give a great deal higher voltage sensitivity in the simple circuit than is usually obtained. It is further proposed to demonstrate a method of using large input resistances with radio valves of the screen grid type.

Voltage Sensitivity as a Function of the Filament and Plate Potentials

The sensitivity to voltage of the system shown in Fig. 1A is given by

$$S_v = G_m S_g,$$

where S_v is the voltage sensitivity, G_m the mutual conductance and S_g the galvanometer sensitivity.

In this simple circuit the galvanometer sensitivity must be adjusted to suit the plate current and in the work to be described was always kept such that the initial plate current caused a 50 percent deflection of the total scale length. In computing the sensitivity in amp./mm a total scale length of 50 cm, was employed, the value of the plate current used being the lowest it was possible to obtain and remain in the region of linear mutual conductance.

Under these conditions a factor proportional to the voltage sensitivity will be given by substituting the reciprocal of the plate current for the galvanometer sensitivity in the above equation. However, while the mutual conductance is determined by the mechanical constants of the valve it is also a function of the filament and plate potentials, in general decreasing as they decrease. The sensitivity of the galvanometer on the other hand being inversely proportional to the plate current increases with lower operating potentials, so that the maximum voltage sensitivity will be obtained when the quotient of the mutual conductance by the plate current is a maximum. Examination of this quantity has been made and the following data will show clearly that the galvanometer sensitivity increases more rapidly than the mutual conductance decreases, as the operating potentials are lowered. The tube employed in the investigation was a UX 222, which is of the four element screen grid type, with the control grid at the apex, which gives the greatest possible insulation between this grid and filament, a factor of the utmost importance if a high input resistance is to be used, as has been pointed out by others.[1, 2]

Table I. *Operating constants of a UX 222.*

Fil. volts	Plate volts	Screen volts	Plate current (micro-amp.)	Mutual conductance
3.3	90	45	925	280
3.3	90	0	10	25
3.3	90	tied to plate	4300	560

For alternating-current amplification the manufacturers specify a plate potential between 90 and 135 volts and a screen grid potential of 45 volts, but the tube may, of course, be operated with the screen grid connected to the filament, at a potential positive to the filament or tied to the plate. The data of Table I have been obtained in this laboratory for these three methods of operation.

In order to reduce the number of necessary observations in examining the variation of voltage sensitivity with operating potentials, grid potential *vs.* plate current curves were first

[1] Nottingham, J. Frank. Inst. **209**, 287 (1930).
[2] H. Nelson, Rev. Sci. Inst. **1**, 281 (1930).
[3] R. D. Bennett, Rev. Sci. Inst. **1**, 427 (1930).
[4] Metcalf and Thompson, Phys. Rev. **36**, 1489 (1930).

run for different filament and plate potentials with the screen grid tied to the plate.

The effect of decreasing the filament voltage at any one plate potential was in general to increase the voltage sensitivity. The effect is most marked at the extremities of the permissible range of variation and thus in order to obtain maximum efficiency with stability, it is desirable to operate at potentials slightly in excess of the lower extreme.

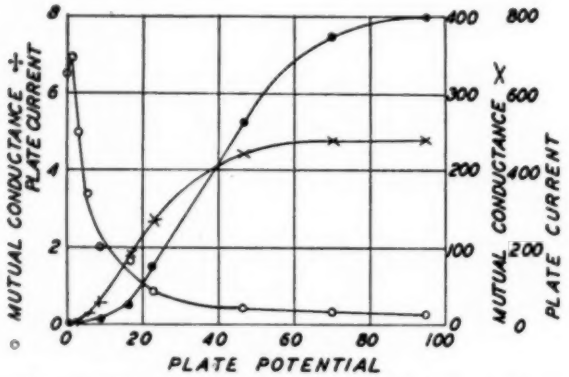

FIG. 2. Data showing how the sensitivity to voltage, measured in millimeters per volt, increases with decreasing operating potentials of the valve. The mutual conductance divided by the plate current is proportional to the sensitivity in millimeters per volt.

Having determined the most desirable filament voltage for any plate potential an examination to determine the most efficient plate voltage was carried out, the results being shown in Fig. 2, where the plate potential is plotted against the quotient of the mutual conductance by the plate current. These curves show that the lower the plate voltage the greater the sensitivity of the unit save with zero volts on the plate where the sensitivity drops off slightly. With the particular tube used to determine the foregoing data the voltage sensitivity was found to rise from 3×10^{-2} volt/mm at 90 volts on the plate to 5×10^{-4} volt/mm with a plate potential of 1.5.

CURRENT SENSITIVITY

Tube as a triode

The sensitivity to current S_c is given by

$$S_c=[R/(1+R/R_g)]S_v,$$

where R_g is the grid-filament resistance and R the magnitude of the input resistor.

It will be apparent from this expression that the sensitivity to current will increase directly with R provided this quantity is small relative to R_g. Moreover under this condition it is independent of the sign of R_g; that is, it does not matter whether an electron or positive ion grid current is employed. The upper limit to the value of R that may be used is, at present, placed by the magnitude of the resistances available. These may be obtained commercially having values as great as 10^{11} ohms, so that in order to obtain the maximum effect the grid-filament resistance of the tube should be not much less than 10^{13} ohms.

Lowering filament and plate potentials to increase the grid-filament resistance is not new having been carried out with signal success by Metcalf and Thompson,[4] in producing a vacuum tube suitable for use as an electrometer. These investigators employing low potentials and aided with a positive space charge grid secured grid-filament resistances as high as 10^{16} ohms, with a specially constructed tube.

General experience with amplifiers leads one to conclude that better results are obtained by using as low an input resistance as possible. For this reason we chose to set the operating constants of the valve to give maximum voltage sensitivity and utilize the existing grid-filament resistance, rather than attempt to improve this quantity at the expense of the voltage sensitivity. Accordingly these resistances were measured for the same filament and control grid voltages as those used to determine the data for Fig. 2. With plate potentials above 15 volts the grid current was found to lie in the positive ion region the resistance rising from 5×10^{9} ohms with 96 volts on the plate and 2.3 on the filament, to 5×10^{10} ohms with a plate potential of 15 and a filament potential of 1.6 volts. Below 15 volts the negative bias necessary for linear mutual conductance was not sufficient to operate the tube in the positive ion region. Accordingly below this value the resistance dropped considerably as the positive ion is smaller than the electron current on any one grid current curve, and at 10 volts on the plate it was found to be 4×10^{9} ohms or approximately the same value as that for 90 volts when in the positive ion section, though it increases as the potentials are lowered farther.

Tube as a screen grid

The large drop in the grid-filament resistance resulting from the necessity of working on the electron section of the curve with low operating potentials led to an examination of the effect of the screen grid on the plate current curve.

(1) *Plate at zero potential.* A family of grid potential *vs.* plate current curves were run for different screen grid potentials, there being no battery in the plate circuit. These are plotted in Fig. 3, while in the upper left-hand corner is

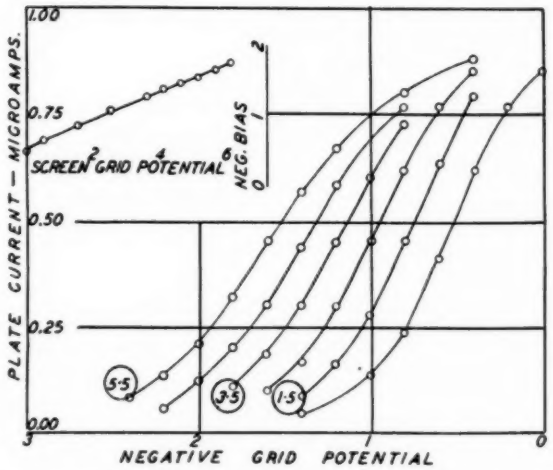

FIG. 3. These curves show that increasing the screen grid potential moves the grid potential *vs.* plate current curve to the left. The encircled values are those of the screen grid. The applied plate potential was zero.

inset a graph showing how the curves shift to regions of lower negative bias with increasing screen grid potential. The shift is directly proportional to the applied potential. It will be apparent from an examination of this family of curves that increasing the screen potential does not alter the value of the maximum mutual conductance but that it does cause this section of the curve to shorten. An upper limit is thus placed on the value of the potential that may be employed and further examination showed this value to be slightly in excess of 6 volts.

The manner in which the screen grid affected the grid current curve was then examined and this curve was found to be moved toward the origin as the screen potential was increased, not, however, to the same extent that the plate current curve was moved away. The above two findings show the value of employing a screen grid. Since grid currents decrease with increasing negative bias, the larger the screen grid potential the greater the grid-filament resistance, an upper limit being placed by the tendency of the region of linear mutual conductance to disappear with higher screen voltages. The grid-filament resistance measured with the maximum permissible screen grid value was found to be somewhat in excess of 2×10^{12} ohms and still to lie in the electron region. The constants of a current amplifier constructed on the above lines are:

Screen grid	6.0 volts
Filament	2.0 volts
Input resistance	10^{19} ohms
Plate	0
Grid filament resistance	2×10^{12} ohms
Control grid potential	-2.0 volts
Current sensitivity	4×10^{-13} amp./mm
Mutual conductance	0.36×10^{-6} amp./volt
Voltage sensitivity	4×10^{-3} volt/mm

(2) *Higher plate potentials.* With screen grid potentials in excess of those of the plate the value of the plate potential, provided it was not zero, was found to have little effect on the plate current curve and as the following work shows it necessary to have screen potentials in excess of six volts, the value of the plate potential will make little difference provided it is below this figure. Accordingly the lowest convenient potential available, that of a single dry cell, was adopted.

The effect of the screen potential on the plate current was found to be different from that when no plate potential was used. As the screen grid was made more positive both the plate current and mutual conductance increased. An examination of the relative rates of increase showed that with higher values of the screen the ratio of the mutual conductance to the plate current decreased. Hence, provided the plate potential is less than the screen grid, the screen grid in a four element tube alters the plate characteristics in the same manner as did the plate potential discussed in the first part of this paper. Thus, as before, in order to retain high-voltage sensitivity, low screen grid potentials must be employed to give a low plate current if one is to work on the linear portion

of the curve. The use of a high screen potential to obtain a high grid-filament resistance is thus prohibited. This condition led to an examination of the possibility of working on the lower curved section of the plate current curve.

The values of the mutual conductance and plate current for maximum voltage sensitivity were obtained by running a plate current curve with the screen at zero potential. The screen was then given various positive values and the corresponding plate curves run over the same range of plate current as in the first instance, the galvanometer thus being kept at a constant sensitivity. The resulting family of curves shown in Fig. 4 are run for screen potentials between

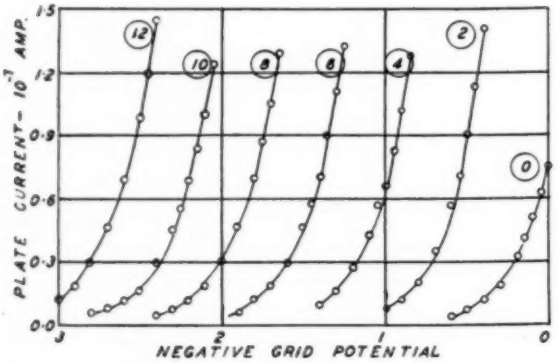

FIG. 4. These curves demonstrate the same phenomenon as Fig. 3. The applied plate potential in obtaining these curves was 1.5 volts. Increasing the plate potential up to six volts makes no appreciable difference to the curves.

0 and 12 volts and it will be seen that they are identical in shape, which gives the same end result as was obtained in the previous section where no plate battery was employed. That is, increasing the screen grid does not alter the voltage sensitivity, provided that in this case the negative bias is increased sufficiently to offset the resulting increase in plate current, which means that the valve is not operated on its linear section of plate current.

Apparently then, operating the valve in this manner, that is on the negative end of the plate current curve, allows the same ratio of slope to plate current to be obtained with high screen grids as with low and the high input resistance resulting from high screen grid values is retained.

In Fig. 5 is shown a full grid potential *vs.* plate current curve with 12 volts on the screen grid, while the lower section is replotted as

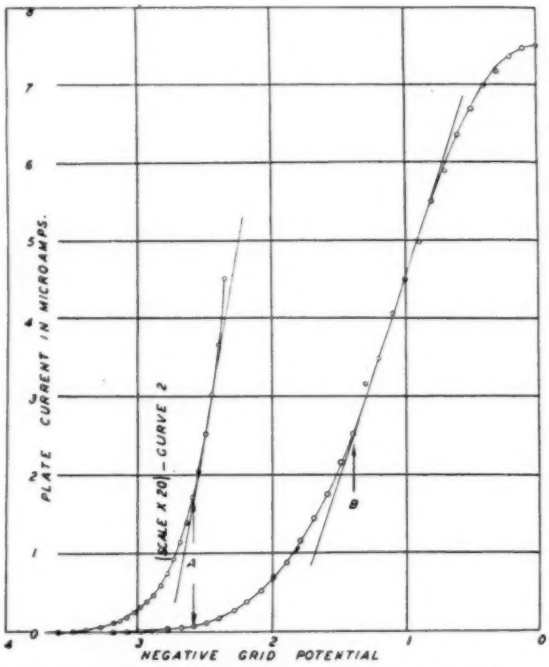

FIG. 5. The plate current characteristic of a high sensitivity direct-current amplifier. For maximum sensitivity with the simple circuit the valve is operated at point *A*, for balanced circuits at the point *B*. Curve 2 is the lower section of curve 1 plotted with a larger vertical scale.

curve two in the same figure, with the vertical scale increased twenty-fold. The constants of this particular amplifier and others with lower screen grid potentials are given in Table II.

TABLE II. *Operating values for high sensitivity d.c. amplifiers.*

Constants	
Filament potential	1.25 volts
Plate potential	1.5
Galvanometer sensitivity	2.8×10^{-10} amp./mm
Voltage sensitivity	8×10^{-4} volt/mm
Plate current	0.07×10^{-6} amp.
Mutual conductance	0.35×10^{-6} amp./volt

Variables		
Screen grid potential	Grid-filament resistance	Maximum input resistor
12	1×10^{14} ohms (positive ion)	10^{12} ohms
10	6×10^{13} ohms (positive ion)	6×10^{11} ohms
8	1.2×10^{13} ohms (electron)	10^{11} ohms
6	9.8×10^{12} ohms (electron)	10^{11} ohms

In conclusion it may be said that ordinary radio valves are quite satisfactory for many types of direct-current amplification, provided suitable operating constants are used. The

advantage of the use of the simple over balanced circuits is its simplicity, freedom from drift and irregularities of balance.

When it is desired to use a less sensitive galvanometer in the plate circuit, a high screen grid potential may be employed and the tube operated on the tangential section of the grid potential *vs.* plate current curve, though this entails a certain loss of sensitivity. Balanced circuits may also be employed in this region. When only low input resistors are required the tube works very satisfactorily as a triode. The authors employing an input resistance of 250 $\times 10^6$ ohms, a Leeds and Northrup type 2420 internal reflecting galvanometer and plate current compensation by a dry cell, have used the triode circuit for over six months for the daily measurement of radon seeds. The type 2420 galvanometer is particularly satisfactory for this purpose as the instrument is operated by technicians and will stand a great deal of rough usage.

This work has been carried out in the Radium Laboratory of the Manitoba Cancer Relief and Research Institute, established in the Department of Physics, University of Manitoba, and the authors would like to express their thanks for the courtesies of these institutions.

Minimum Capillary Rise in an Ideal Uniform Soil

W. O. SMITH, *Pittsburgh, Pennsylvania*

(Received March 15, 1933)

The rise, into an ideal uniform soil, of liquid, under the action of capillary forces, differs from the steady flow across the soil. The steady transmission of fluids takes place through the continuous capillaries extending across the soil; the rise, under capillary forces, of liquid is from cell to cell. The hexagonal scheme of grains spaced at a distance $(2r+d)$, where d is a function of porosity, is used as a statistical representation of the soil; and the problem discussed from the standpoint of this packing. The fluid, in its passage through the long capillaries, flows through a cyclic capillary showing definite maxima and minima in each element; and likewise, the rise, from cell to cell, under capillary forces, is through a channel with definite maxima and minima. The minimum opening, of a cell, is the section defined by the plane of centers; the greatest is the section defined by the plane, parallel to the plane of centers, tangent to the grains of the cell immediately over the first cell. The greatest rise, occurs when the minimum opening holds the meniscus and is observed by allowing the liquid to fall through the soil; the least rise should occur when the maximum opening holds the meniscus and should be observed by allowing the liquid to rise through the soil. Wetting phenomena introduce, however, complications affecting the minimum rise. Rings of liquid form, just above the meniscus, around the point of contact of each pair of grains, and carry the rising liquid higher until it attains a position where it is no longer able to reach the rings so formed; equilibrium then prevails at a rise intermediate to the two extremes just defined. The exact conditions controlling the rise phenomena are determined; the approximation, developed for the capillary equation, in an earlier paper, is then used, with these conditions, to calculate the minimum rise. The results are compared with the data given in the earlier paper; good agreement, within the experimental error, is obtained.

THE capillary rise of liquid in an assemblage of uniform spheres, small enough to constitute an ideal soil is, by experiment, found to be variable. The assemblage of uniform spheres, i.e., the ideal soil, will support liquid at a number of different heights above a free liquid surface. When allowed to reach equilibrium by falling the liquid attains its greatest distance above the free surface; if allowed to rise it stops at the minimum height; and, finally, if forced, artificially, to a given position between, maintains the intermediate height; thus multiple positions of equilibrium, all lying between a definite maximum and minimum, exist. A sketch of apparatus, suitable to investigate this phenomena, is shown in Fig. 1a. A is a container for the soil; B is a liquid reservoir; a is a screen, of mesh suitable to keep the soil in the column A above. A stoppered opening C can be used for filling or removing liquid—a siphon is convenient for the latter purpose; c is a vent, sufficiently small to prevent undue evaporation and yet permit atmospheric pressure to prevail over the free liquid in B. The distance of the meniscus, in the sand column A, above the free liquid surface, in B, is the capillary rise. Fig. 1b shows an apparatus more convenient to investigate the maximum rise throughout a long column of sand, but unsuitable for determining the minimum. The stopcock D is convenient for removing liquid, but allows leakage—no grease can be used; hence, if initially the liquid is allowed to rise in A, it is later observed to fall in B until the maximum is reached, after which the liquid system begins to drop as a whole. To proceed with a physical explanation, it is necessary to, first, give a suitable statistical representation for the packing.

The ideal soil can be considered, statistically, as a regular hexagonal array of spheres spaced at the distance $(2r+d)$ required to furnish the observed porosity P; r is the grain radius and d the spacing constant.[1] The quantity $(2r+d)$ is given by

$$(2r+d)^3=4(2)^{\frac{1}{2}}r^3/3(1-P). \qquad (1)$$

Three types of pore cell exist in this packing and occur, moreover, in a definite relative

[1] Cf. Smith, Foote and Busang, Physics **1**, 18–26 (1931); also Smith, Physics **3**, 139–146 (1932).

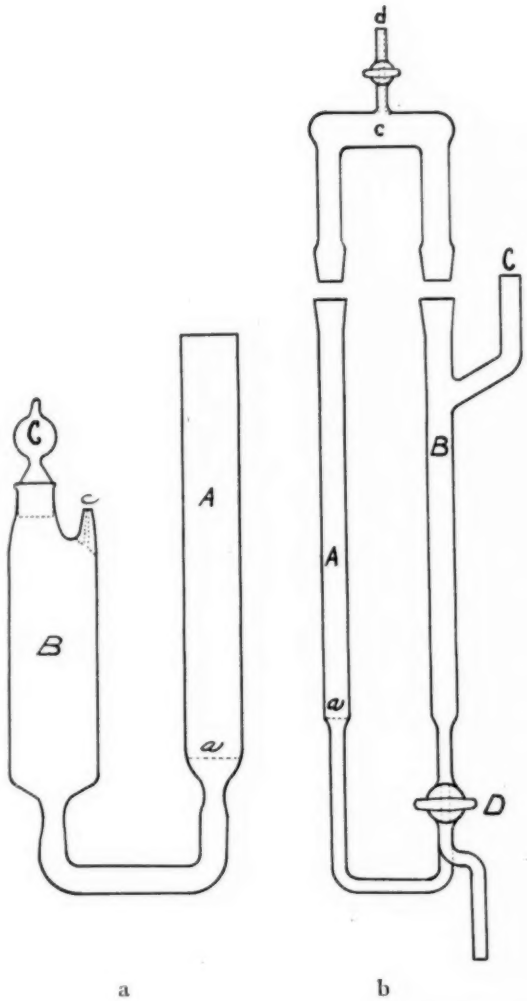

FIG. 1. (a) Tube used to determine rise into granular materials. (b) Tube used to determine maximum rise into granular materials.

frequency. These are shown in Fig. 2 under the letters T, S and R. The unit element, comprising eight grains, is also shown in that figure and permits easy identification of these cell types; the grain triads (1, 3, 8) and (4, 5, 7) form two T type cells; grain tetrads (3, 4, 7, 8), (1, 3, 5, 7) and (1, 4, 5, 8) constitute three S type cells; the exterior faces of the rhombohedral element form six R type cells. These are the only cell types present and are repeated, in the pattern given by the unit element, throughout the packing. The frequency of occurrence, throughout the volume, of each cell type, is that prevailing in the unit element, and since the R cells are shared by adjacent unit elements, these frequencies are observed to be in the ratio

$$n_T : n_S : n_R = 2 : 3 : 3. \qquad (2)$$

n_T, n_S, n_R are, respectively, the numbers of T, S and R cells present.

These cells, finally, are found to be arranged so that three sets of capillaries run, continuously, across the element, and, if the whole packing is considered, these capillaries are found to run continuously throughout its extent. A single set consists of two capillaries; the course of one such set is marked, in Fig. 2, by the rods AB and $A'B'$. The cells bounding these triangular capillaries are either T cells or half-R cells; thus the capillary $A'B'$ progresses through the grains (1, 2, 8), (1, 3, 8) and (3, 4, 5). The triangular cell suffices to calculate the average area of the capillary, and is thus sufficient to determine the steady flow of liquid through the packing. It will be observed that each R cell and each S cell is pierced by two such capillaries—in Fig. 2, capillaries AB and $A'B'$ cross the R cell (1, 2, 7, 8), the S cells (1, 3, 5, 7), (3, 4, 7, 8) and finally the R cell (3, 4, 5, 6).

The cross section of a continuous capillary, if followed along its course, will be found to be cyclic, entering the unit element at a minimum, expanding to a maximum, back to a second minimum, and after another repetition leaving the element at a minimum; this succession is

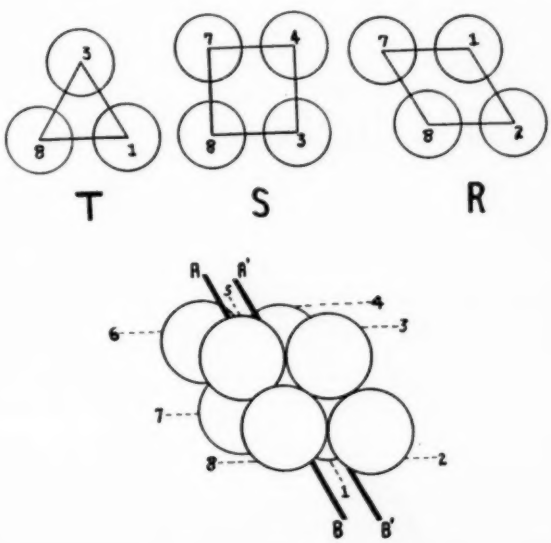

FIG. 2.

repeated from element to element. One of the consequences of such cyclical repetition, in a capillary tube, of a definite maximum and minimum section, is the existence of multiple equilibrium positions.[1] This is in contrast to the rise of liquid in a simple cylindrical tube, where but a single height of liquid is sustained above a given liquid surface. The phenomenon is best understood by considering a capillary composed of a single repeated element. Let the element, as a simple example, be the frustrum of a cone; then the capillary will be composed of a number of these placed end to end along the common axis. The multiple conical tube, thus formed, shows a maximum rise corresponding to the smaller opening of the frustrum and a minimum corresponding to the larger one.[1] Equilibrium is possible in each element lying between these extremes. We are thus led to expect, when capillary rise of liquid is considered, that the cyclic capillaries of the hexagonal packing, such as AB in Fig. 2, would give rise to multiple positions of equilibrium; these positions would show a maximum produced by drainage and a minimum by filling, and if the liquid were, by external means, forced between, intervening positions would be possible.

The system of continuous capillaries suffices for the steady transmission of fluids across the soil; when the packing is once filled, they alone need be considered for steady flow across its interior. This system is, however, not sufficient for the problems of filling and drainage of liquid; all cell types, T, S and R take part in these processes and all must be considered. It is, therefore, since S cells are not found in the triangular capillaries, not sufficient to only consider these capillaries; the maximum and minimum occurring in them cannot account for observed experimental rises in ideal soils.

Whatever the path of the fluid, under capillary forces, it is, nevertheless, from cell to cell, and in each case along the axis (of the cell) defined as the normal to the plane through centers. The channel between any two adjacent cells, is still cyclic, and is repeated throughout the packing. Each cell type shows a definite maximum and a definite minimum section, and these cell types are, moreover, repeated in a definite pattern throughout the hexagonal soil; multiple equilibrium positions should, therefore, exist. The ideal soil should likewise exhibit multiple equilibrium positions, for its piling is regarded as generated from the hexagonal scheme by random distortions, all of which are moderate.

The particular problem is to find the possible heights of the meniscus, when in equilibrium above the free liquid, and it is, for this purpose, sufficient to know the distribution of cells, and the possible positions of the meniscus in each. The minimum opening is seen to lie in the plane of centers, and holds the meniscus when at its greatest distance above the free liquid. The maximum opening lies in the plane, parallel to the plane of centers, and tangent to the grains of the cell immediately over it—in Fig. 2 the maximum opening of the R cell (1, 2, 7, 8) is in the plane tangent to the grains (3, 4, 5, 6) forming the R cell immediately above; the meniscus should occupy this position when at its least distance above the free liquid. It is reasonable, if the meniscus is in an equilibrium position, to suppose the individual cells, T, S and R exist, in the meniscus, in the frequency of their occurrence in the unit element; if the minimum opening of each cell type is occupied then we will have maximum rise, if the maximum opening is occupied the liquid will be at the minimum possible distance above the free liquid. To proceed further, it is necessary to consider the capillary equation.

The general behavior of the soil meniscus has been accounted for and an equation for maximum rise derived, by Smith, Foote and Busang.[1] The results rest on fundamental considerations involving the general capillary equation, the nature of the meniscus-grain contact, and the mode of packing. Consideration of the meniscus-grain contact leads to an approximation of the capillary equation suitable for soils; consideration of the mode of packing, as we have seen, leads to a suitable statistical scheme, and to the reason for the existence of multiple positions of equilibrium.

The general condition for equilibrium of a capillary meniscus is

$$\int \rho g z \cos \phi dS = \int \sigma \cos \theta ds, \qquad (3)$$

where z is the height, above the free liquid, of an

element dS of the meniscus, ϕ the angle which the normal to this element makes with the vertical z-axis, ds an element in the meniscus-grain contour and θ is the angle between the vertical and that normal to ds which is tangent to the meniscus.[1] The integrals extend, respectively, over the entire capillary surface and around the corresponding contour contained within the column of packed spheres. The principal problem, for our purpose, is the application of this equation to the complex soil meniscus. Smith, Foote and Busang[1] found it was, for the purpose of soil problems, sufficient to use, as an approximation of Eq. (3), the equation

$$\rho ghA = \sigma p \cos\theta \tag{4}$$

and we shall adopt Eq. (4), likewise, for the present problem. The rise is then given by $h = \sigma p \cos\theta / \rho g a$. In this approximation (Eq. (4)), the meniscus-grain contour, of a given cell, is an approximate one, supposed to lie in a plane passing through the points of the actually existing sinuous contour, which are closest to the plane of centers. a is the area enclosed by and p the perimeter of the "approximate" meniscus-grain contour. θ is now constant for a given section, and is the angle between the axis of the cell and that normal to the line of contour, of the section, which is tangent to the meniscus —the points of tangency are at those parts of the meniscus where the actually existing contour and the approximate one coincide, namely, at points closest to the plane of centers.

The considerations leading to Eq. (4) were for an extreme case, that of maximum rise involving the minimum pore opening. Its validity was established by considerations given in the paper cited.[1] This equation is, for the present problem, subject to question only on the magnitude of the error arising from distortion of the meniscus. This is greatest, for a given position of the meniscus, in the vicinity of grain contact points, and is greatest, for all positions of the meniscus, when the plane of the meniscus is in the vicinity of the minimum pore opening. It has been shown, in the paper cited,[1] however, that no serious error occurs when the liquid is in the latter position. The effect decreases as the meniscus rises or falls, in a given cell, away from this position, and is, therefore, of even less importance in the application of Eq. (4) to the minimum rise. It should be observed, finally, that each plane in the interval between the maximum and the minimum opening, is a possible plane of projection of the meniscus, for some particular rise, produced generally by external means, into the soil.

The quantity $\rho ghr/\sigma$ is more convenient for calculating the rise, if the density ρ and surface tension σ of the liquid, the grain radius r and g the acceleration of gravity are known. We have, from Eq. (4)

$$\rho ghr/\sigma = rp \cos\theta / a. \tag{5}$$

This quantity has the further advantage that it is dimensionless and will be found to depend only upon the porosity. p is the perimeter, and a the area of the particular section involved. θ, if, as in the paper cited,[1] we suppose that complete wetting exists, is equal to the angle, for a given cell, between the radius vector, from a given grain center to the intersection of that grain with the section of the pore under discussion, and the plane through centers. The quantity $p \cos\theta$ is proportional to the upward surface force, the quantity a is proportional to the downward force exerted by the weight of the liquid column. The values of the quantities $p \cos\theta$ and a, for each of the cell types, must, to find the average value of $p \cos\theta / a$ for the whole soil, be weighted in the proportion of the respective cell frequencies given by Eq. (2). We thus find

$$\frac{\overline{p\cos\theta}}{a} = \frac{2p_T \cos\theta_T + 3p_S \cos\theta_S + 3p_R \cos\theta_R}{2a_T + 3a_S + 3a_R}. \tag{6}$$

From Eqs. (5) and (6)

$$\overline{\rho ghr}/\sigma = \overline{rp\cos\theta}/a. \tag{7}$$

Eq. (7), provided the perimeters and area, and appropriate values of θ are known, enables one to calculate the minimum, maximum, or the rise to an intervening position. Table I shows, the values of p and a for each cell of the hexagonal soil.

θ, for the maximum rise, has, for each cell, the value zero; the meniscus lies in the plane of

TABLE I. *Summary of values of p and a for T, S and R cells.*

Cell type	p	a
T	$\pi r \cos\theta_T$	$(2r+d)^2(3)^{\frac{1}{2}}/4-\pi r^2\cos^2\theta_T/2$
S	$2\pi r\cos\theta_S$	$(2r+d)^2-\pi r^2\cos^2\theta_S$
R	$2\pi r\cos\theta_R$	$(2r+d)^2(3)^{\frac{1}{2}}/2-\pi r^2\cos^2\theta_R$

centers. We find, on substituting $\theta=0$ in Table I, using the values so found in Eq. (6), and applying Eq. (7), that the maximum rise, h_f, is, when $(2r+d)$ is replaced by its value in terms of P from Eq. (1), given by[1]

$$\rho g h_f r/\sigma = 2/\{[0.9590/(1-P)^{\frac{1}{3}}]-1\}. \quad (8)$$

The values of θ, for the greatest opening are easily found. The greatest opening, it will be recalled, is in the section, parallel to the plane of centers and tangent to the grains of the cell immediately above. For the R cell, we need only consider the tetrahedron formed by three adjacent grains of the cell and one, of the cell above, which interlocks with them—cf. Fig. 5. The distance l_R of the maximum section above the plane of centers is $l_R=(2r+d)(2/3)^{\frac{1}{2}}-r$. θ_R is found to be given by $\cos^2\theta_R=(r^2-l_R^2)/r^2$. For the S cell, we consider the pyramid formed by the grains of the cell as base, and one of the cell above as vertex. The distance of the maximum section above the plane of centers is $l_S=(2r+d)(2)^{\frac{1}{2}}/2-r$. θ_S is given by $\cos^2\theta_S=(r^2-l_S^2)/r^2$. Finally, the value of θ_T for the T cell is identical with that of θ_R for the R cell. Using these values of θ in Table I, and substituting the values of p and a so found in Eq. (6), we find, from Eq. (7), on replacing $(2r+d)$ by its value from Eq. (1), that the absolute minimum rise h_r can be obtained as follows: from Eqs. (6) and (7)

$$\rho g h r/\sigma = 2/\{[6.740/(1-P)^{\frac{1}{3}}(4\cos^2\theta_R+3\cos^2\theta_S)]-1\};$$

from the above values of $\cos^2\theta$ we find

$$(4\cos^2\theta_R+3\cos^2\theta_S) = 19.50/(1-P)^{\frac{1}{3}}-13.64/(1-P)^{\frac{1}{3}};$$

and finally

$$\rho g h_r r/\sigma = 2/[\{0.4940/[1.429(1-P)^{\frac{1}{3}}-1]-1\}]. \quad (9)$$

The minimum rise, given by Eq. (9) cannot, in general, be observed because of an accompanying phenomena, the formation of liquid rings above the meniscus; these rings are, up to a certain height above that given by Eq. (9), capable of destroying the equilibrium. The explanation involves the mechanism of formation of the rings, their effect on the meniscus, and the limiting height at which they can no longer affect the meniscus. The origin of the rings is vapor condensation; vapor ahead, in the free pore space, condenses on the grains, and especially on those grains just above the meniscus. The liquid so condensed accumulates in rings around the contact points of each pair of adjacent grains; it must accumulate around the contact points rather than in a uniform layer over the grains, otherwise the surface energy of the liquid, thus condensed, would not be a minimum. The rings, once formed, will continue to grow until their curvatures attain values required by the vapor pressure prevailing in the pore space just over the ring-meniscus. The criterion for the proper curvatures is furnished by Kelvin's theorem.[2] When the soil-meniscus is in the position given by Eq. (9), and this, it should be noted, is close to the top of the cell, the liquid distributed in the rings in the grain layer, just above, will increase by condensation, and each ring will grow. The ring-meniscus will advance outward from the contact point and finally meet the soil-meniscus; when it does, the soil-meniscus is contacted with, and rises into, the next layer of grains. The process will continue until the rings cease to grow, and are no longer able to reach the meniscus; equilibrium will then prevail.

The meniscus and rings, just above, will be in equilibrium when their vapor pressures are equal—neglecting small distances of the order of a grain radius. From Kelvin's investigation[2] the vapor pressures of the ring and meniscus, just below, are equal when their curvatures are equal. The meniscus will, in any case, advance until this condition is satisfied; when it is, equilibrium will prevail. The meniscus will, when these conditions are first satisfied, be at its minimum distance above the free liquid, and,

[2] W. Thomson, Phil. Mag. [4] **42**, 448 (1871).

further, will be in a layer of grains where it is just unable to meet the rings immediately above. For positions of the meniscus, above the layer of grains corresponding to minimum rise, the meniscus and ring will still have equal curvatures, but they will be separated by distances which increase as the meniscus rises further into the soil. Positions above the minimum will be stable as long as there is a cell section capable of supporting a meniscus; the limiting position is that of maximum rise, and occurs when the smallest cell opening, that in the plane of centers, is occupied. These relations are shown for the hexagonal soil in Fig. 3. For the purposes of this soil we define a contact point as the point on the axis of two grains equidistant from each.

The actually observed minimum rise, occurring when the meniscus is just unable to meet the ring in equilibrium with it, can be ascertained; and for this purpose we shall first consider the portion of the meniscus just over the contact point of a pair of grains of the cell. We mention that the meniscus is most elevated here, for the cell is narrowest; also, it will, in general, in this vicinity just above a contact point, first reach the ring. It has, moreover, just over the contact point, a geometrical form closely approximating that of the ring, and its two principal curvatures, in this region, are, to a close approximation, respectively equal to the corresponding curvatures of the ring. The last statement is, in reality, an assumption, but is justified as an approximation if we assume the capillaries, as in our problem, are small, and note that both capillary surfaces, the ring-meniscus and the soil-meniscus, in the region over a contact point, are solutions of the same partial differential equation for approximately the same boundary.

The last assumption of equal curvatures and similar shape, over a contact point, for ring and soil-meniscus, enables us to fix the point where the ring and soil-meniscus are just unable to meet. It is observed, first, if spaced hexagonal packing is considered, that regardless of cell type, the part of the meniscus over a contact point, and the ring are always associated with a three grain cell, as shown in Fig. 3—in the triangle of centers each triangle is 60° and each edge is $(2r+d)$. We can, further, represent the curve of intersection of the grain with the part of the meniscus above the contact point by the arc of a circle. The ring contour can, likewise, be represented by a circle. These two circles have, by the above assumption, equal radii, and will meet first in the plane of centers of the three-grain cell. The points a and b of Fig. 4 are two such points where the circles just touch. The ring circle R and the meniscus circle R' meet at a and lie in the plane AOB. A and B are, for practical purposes, contact points of two adjacent grains, which together with the grain shown—center at O—form a typical three-grain cell. The lower diagram of Fig. 3 also shows these points. The angle AOB, is bisected by the line Oa, i.e., the line from the grain center to the common point of tangency of the circles. The axis of the ring is the line joining the centers of the two grains supporting it; the angle ψ between the axis and the radius vector from

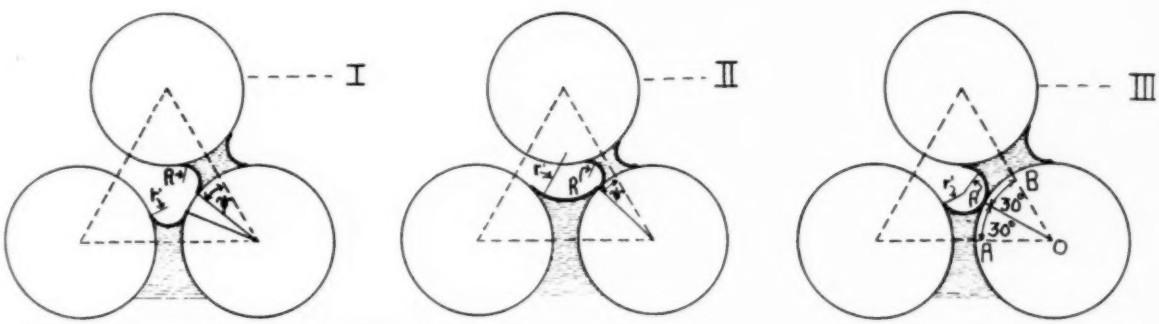

FIG. 3. Relative positions of ring- and soil-meniscus with respect to the minimum observable rise: I—above this position; II—below; III—at the position of minimum observable rise. R and r' are curvature-radii, in the plane of the figure, for the ring- and soil-meniscus, respectively.

the center of a grain to the edge of the ring on that grain is easily seen, for the particular ring which is just unable to meet the meniscus, to be given by $\psi = 30°$. We have thus found the size of the ring which determines minimum rise. Closer consideration of this ring and its relation to the meniscus-grain intersection will enable us to choose, for each cell type, the plane of projection of the meniscus appropriate to minimum rise.

If we examine the meniscus-grain contour between the consecutive points a and b where it meets the ring, we see that it can be considered to follow closely below the contour of the ring—cf. Fig. 4—provided the capillary size is not too large. Eq. (4) requires us to take the point of the meniscus-grain contour closest to the plane of centers, as lying in the plane of projection of the meniscus; it was shown in the earlier paper[1] that the plane of the meniscus, for the purpose of Eq. (4) passes through this point, and is parallel to the plane of centers. We shall consider it a sufficient approximation to take the plane of the meniscus as passing through the point of the ring, closest to the plane of centers; the corresponding point of the meniscus is just below and close in its position to it. Fig. 4 shows these relations; S is the meniscus-grain contour, S' is the "approximate" contour and c is the point of the ring closest to the plane of centers AOC. It remains to find these positions for each cell type.

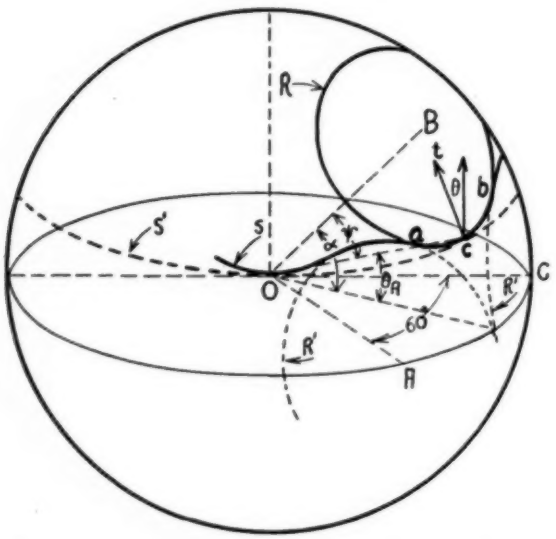

FIG. 4. Relative positions of ring-grain and meniscus-grain intersections for the minimum observable rise; S is meniscus-grain contour; S' is the intersection of the approximate meniscus with the grain; R is the ring-grain intersection. The two circles marked R' are those coinciding, just over contact points, with S, and meet the ring R at points a and b.

We observe from Fig. 5 that the angle θ_S, measured from the plane of centers of the S cell,

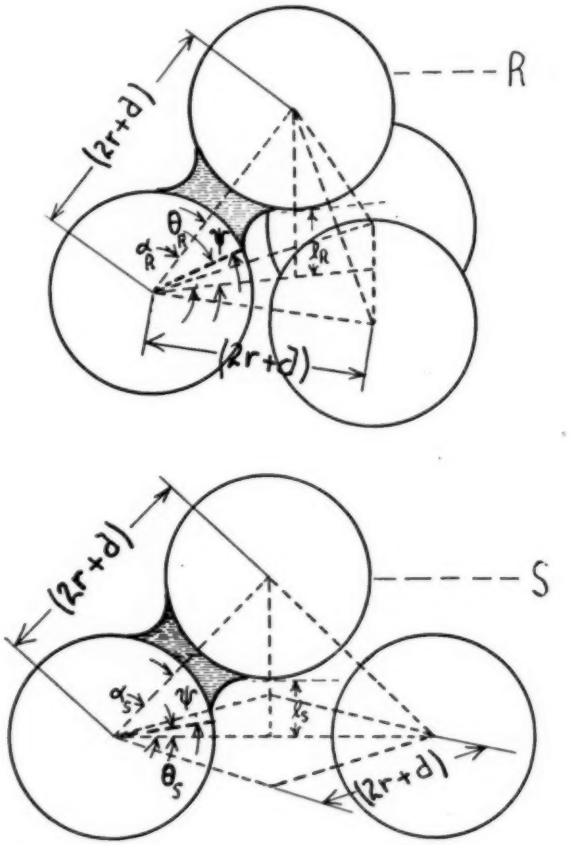

FIG. 5. R—Elementary tetrahedron for the R-cell. S—Elementary pyramid for the S-cell. $\alpha_S = 45°$; $\alpha_R = 54° 44'$ $\psi = 30°$; $\theta_S = 15°$; $\theta_R = 24° 44'$.

and included between this plane and the radius vector, from the center of a given grain of the cell to the lowest point of the ring, is given by $\theta_S = \alpha_S - \psi$; $\alpha_S = 45°$; $\psi = 30°$. For the R cell—cf. Fig. 5—we find $\alpha_R = \cos^{-1}[(2r+d)(2/3)^{\frac{1}{2}}/(2r+d)]$; $\alpha_R = 54° 44'$; $\psi = 30°$; and $\theta_R = \alpha_R - \psi = 24° 44'$. We have also $\theta_R = \theta_T$. If, finally, we use these values in Table I, we find from Eqs. (1), (6) and (7) that h_m, the minimum observable rise, is given by

$$\rho g h_m r/\sigma = 2/\{[1.105/(1-P)^{\frac{1}{3}}]-1\}. \quad (10)$$

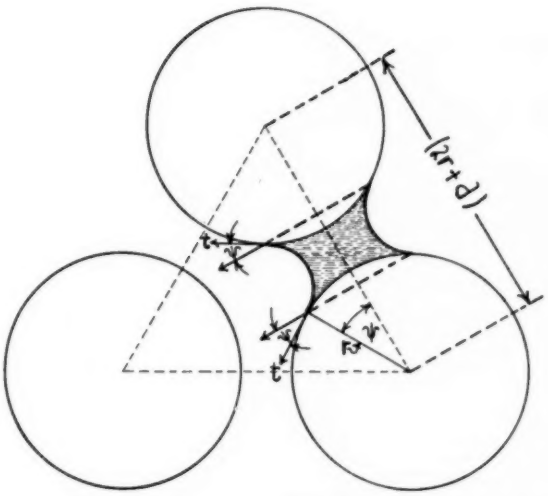

FIG. 6. This diagram shows the direction of the capillary forces acting at the ring-grain contour. t is the tangent to the ring meniscus at this intersection; ψ is the angle of the ring.

If we consider the rings alone, each having a value of $\psi = 30°$, regardless of cell type as above, we can derive an equation which agrees closely with Eq. (10). We observe that if there is true equilibrium, and if, further, the ring liquid body is placed in contact with the bulk of liquid under the meniscus; e.g., by a pipe running through one of the grains about which the ring is formed, one end opening at the point of contact and the other beneath the soil-meniscus, then neither the ring-meniscus nor the soil-meniscus should be disturbed. In that case we may apply Eq. (3) and as an approximation we find; cf. Fig. 6:

$$\frac{\rho g h}{\sigma} = \frac{2(2\pi r \sin\psi \cos\psi)}{2\pi r \sin\psi[(2r+d) - 2r\cos\psi]},$$

where h is the height of the ring above the free liquid. Replacing $(2r+d)$ by its value from Eq. (1) we find, remembering that $\psi = 30°$, for minimum rise

$$\rho g h_m r/\sigma = 1/\{[1.044/(1-P)^{\frac{1}{3}}] - 1\}. \quad (11)$$

An extended series of data was given by Smith, Foote and Busang,[1] for both maximum and minimum values of $\rho ghr/\sigma$ as a function of the porosity P. Carefully graded sands and round glass beads were used. The glass pearls were closely spherical, and similar to those used by Green and Ampt[3] in their investigations on the capillary flow through ideal soils. Tables IIa, b show the data and are those used to plot the curves of the earlier paper. These data, as well as Eqs. (9), (10) and (11) are plotted in Fig. 7. Eq. (9) is seen to lie considerably below the observed data; Eq. (10) fits closely; Eq. (11) presents approximate agreement, with the values for $\rho ghr/\sigma$ slightly higher than those given by Eq. (10).

The value of ψ, required for agreement with the data as close as that shown by Eq. (10) is about 31°. The proper ring value of ψ is slightly greater than 30° as the following considerations

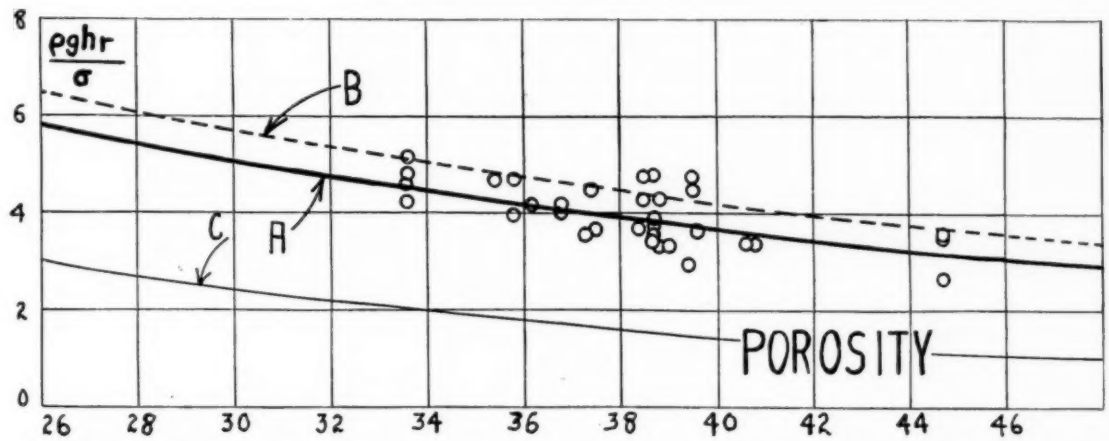

FIG. 7. Plot of $\rho ghr/\sigma$ as a function of porosity: Curve A represents Eq. (10); curve B, Eq. (11); curve C, Eq. (9). The data are those given in Tables IIa, b.

[3] Green and Ampt, J. Agricultural Science, 5, No. 1 (1912–1913).

TABLE IIa. *Summary of experimental values of* $\overline{\rho ghr/\sigma}$ *for glass pearls.*

Porosity P	Grain radius r cm	Capillary liquid	$\overline{\rho ghr/\sigma}$ Maximum rise		$\overline{\rho ghr/\sigma}$ Minimum rise		
			Obs.	Eq. (8)	Obs.	Eq. (10)	Eq. (11)
0.447	0.0316	Carbon tetrachloride	4.70	4.70	3.53	3.16	3.68
.447		Lubricating oil	4.60	4.70	2.64	3.16	3.68
.447		Crude petroleum	4.29	4.70	3.49	3.16	3.68
.408		Carbon tetrachloride	4.88	5.50	3.32	3.55	4.12
.396		" "	5.40	5.80	3.60	3.70	4.25
.390		Xylene	5.35	5.96	3.50	3.78	4.30
.388		Water	5.30	6.00	3.32	3.80	4.33
.387		Carbon tetrachloride	6.06	6.04	3.88	3.82	4.35
.387		" "	5.91	6.04	3.72	3.82	4.35
.387		Toluene	5.96	6.04	3.40	3.82	4.35
.387		Benzene	5.69	6.04	3.55	3.82	4.35
.384		Acetylene tetrachloride	6.04	6.10	3.67	3.87	4.40
.373		Carbon tetrachloride	6.49	6.42	3.54	4.00	4.41
.368		Water	6.42	6.56	4.16	4.08	4.62
.368		Benzene	6.10	6.56	4.00	4.08	4.62
.358		Zephyr oil	6.51	6.90	3.97	4.20	4.78
.358		Alcohol	6.18	6.90	4.69	4.20	4.78
.375	0.0323	Carbon tetrachloride	5.54	6.38	3.66	3.98	4.52
.394	0.0246	Toluene	—	—	2.92	3.72	4.28

TABLE IIb. *Summary of experimental values of* $\overline{\rho ghr/\sigma}$ *for graded sands.*

Porosity P	Grain radius r cm	Capillary liquid	$\overline{\rho ghr/\sigma}$ Maximum rise		$\overline{\rho ghr/\sigma}$ Minimum rise		
			Obs.	Eq. (8)	Obs.	Eq. (10)	Eq. (11)
0.374	0.0443	Carbon tetrachloride	6.95	6.40	4.45	3.99	4.50
.374		" "	7.23	6.40	4.45	3.99	4.50
.374		Xylene	6.04	6.40	3.65	3.99	4.50
.362		Carbon tetrachloride	6.86	6.77	4.12	4.13	4.68
.358		" "	7.17	6.88	4.69	4.20	4.73
.354		Water	6.94	7.00	4.62	4.26	4.80
.336		Alcohol	7.49	7.60	4.78	4.50	5.07
.336		Carbon tetrachloride	7.62	7.60	5.18	4.50	5.07
.336		Dearboline	7.22	7.60	4.59	4.50	5.07
.336		Zephyr oil	7.46	7.60	4.20	4.50	5.07
.406	0.0135	Carbon tetrachloride	5.36	5.56	3.40	3.58	4.10
.395		Kerosene	6.05	5.82	4.73	3.71	4.22
.395		"	6.05	5.82	4.49	3.71	4.22
.388		Xylene	—	—	4.26	3.80	4.33
.387		Zephyr oil	7.20	6.00	4.75	3.81	4.35
.385		Carbon tetrachloride	7.36	6.10	4.72	3.85	4.39
.385		Benzene	6.72	6.10	4.27	3.85	4.39

show. If any given ring, just above the soil meniscus were displaced slightly and made to touch and merge with the soil-meniscus below, the liquid, above the contact point of the original ring, would retain its shape, but would be pulled slightly toward that point. The general behavior of the soil meniscus over contact points is similar. The ring corresponding to this region is slightly smaller than the free ring above. For an equilibrium determined by the inability of the two menisci, free ring and soil-meniscus, to just meet, we can conclude that the free ring has a value of ψ a little greater than 30° and the ring coinciding with the part of the soil-meniscus over a contact point has a value slightly less than 30°. We thus see, empirically, the limits of validity of our approximation on similar form and equal curvatures for the free ring and part of the soil-meniscus over a contact point. This argument is, for the

hexagonal soil, however, subject to further examination; for rings with a value of ψ greater than 30° will overlap and combine into more complicated patterns.

It should be expected, on the basis of the theory here presented, that maximum rise and equilibrium will be attained in a much shorter time than that required for minimum rise and equilibrium. The rise depends, at least in its final stages, upon the time of growth of the rings; but not so for the maximum rise attained by the falling liquid, for no rings are involved. This behavior appears to be borne out experimentally.

Records of the Effective Height of the Kennelly-Heaviside Layer

G. W. KENRICK, *Department of Electrical Engineering, Tufts College, Massachusetts*

(Received March 6, 1933)

IT is the purpose of this note to show characteristic changes in the effective height of the Kennelly-Heaviside layer recorded photographically with recently developed equipment. Space does not permit a description of this equipment here, but such a description should be available in print by the time this note appears.[1] Some time will elapse before the data accumulated, by using these new methods, will permit a discussion of seasonal and other long periodicities, but many of the diurnal characteristics disclosed during the last winter appear sufficiently typical to warrant a report at this time, particularly as Dr. E. O. Hulbert finds references to these data helpful in connection with a discussion of radio skip distance now in preparation.

Fig. 1 shows records of the effective layer height at Boston, Massachusetts, from February 16–18, 1933, and from February 26–27, 1933. The records are produced by the successive motions of a light beam from bottom to top of the figures as shown. The nearly straight horizontal lines are due to the transmission of a very short dot over the ground path, which is only about 10 km in length, while the variably spaced lines above are due to waves returned from the Kennelly-Heaviside layer. The group retardations of the sky waves are subject to slow diurnal changes and the resulting figures may conveniently be viewed as Cartesian plots of layer height as a function of time, where the straight lines produced by the ground wave transmission are taken as origin lines, and it is noted that multivalued heights, when shown as simple multiples of each other, are multiple reflections (or refractions). This does not apply, however, to "splits" and multivalued heights not in simple relation.

The 2050 kc records show clearly the so-called "*E*" and "*F*" regions of ionization (at effective heights of approximately 100 km and 250 km) and also the somewhat abrupt transition between these heights during the diurnal cycle.[2] A reduction in intensity due to absorption frequently masks the exact time of transition, but on the days shown it apparently occurs between 7 and 8 A.M. from *F* to *E* and from 4 to 5 P.M. from *E* to *F*. The day *E* layer appears but faintly, due, perhaps, to absorption. The time of appearance and disappearance of the layers (but not their effective heights) is, of course, somewhat a function of transmitting set power and receiver gain. In the records shown the transmitting power was about 200 watts and high gain receivers were used. These sets were operated at full gain in the first two records shown, which accounts for the dark background, indicating that the sensitivity recorded went below the disturbance level. Thus, because of the randomness of the disturbance encountered, recording may be carried on at amplifications beyond those at which the pulses can be distinguished on visual inspection because of the tendency of the photographic film to integrate the light received from the synchronized pulses, but not the random noise. Too great gain, however, of course results in too dark a background to permit faint reflections to be distinguished. Under the conditions of these recordings it will be noted that the layer disappeared on the night of February 17–18 in 2050 kc, but persisted fairly consistently, although somewhat weakly, during the night of February 16–17. The record of February 26–27 shows the effects as observed at lower gain. In the case of nearly all the records, a tendency to decreased effective heights and stronger reflections shortly after midnight but long before dawn is noted (see the February 17–18 record). This sometimes results in a minimum height at approximately 3 or 4 A.M.

[1] Kenrick and Pickard, Proc. I.R.E. **21**, April, 1933.

[2] Gilliland, Kenrick and Norton, Proc. I.R.E. **20**, 286–309 (1932).

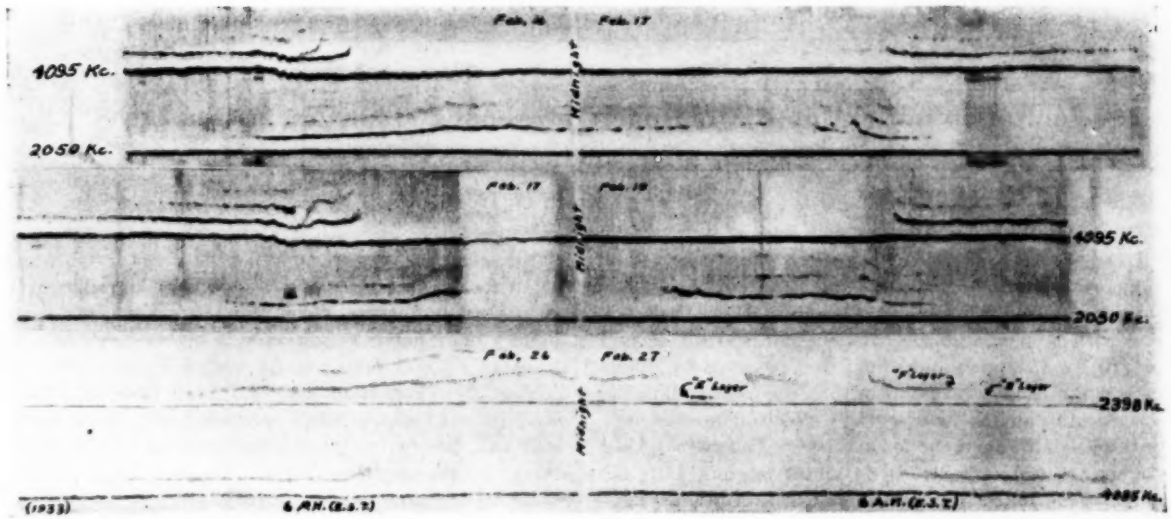

FIG. 1. Record of effective height of the Kennelly-Heaviside layer. (Ordinate scale linear and same for all traces.) Midnight height February 16–17 is indicated as 350 km for 2050 kc on the record shown. Noon height, February17, is indicated as 280 km on 4095 kc.

and sometimes E layers appear at this period as is shown for the record of February 26–27. While several explanations of these phenomena (which are apparently rather consistently observable) are possible, they seem to indicate a definite increase in ionization between midnight and dawn.

The 4095 kc records clearly show a number of multiple reflections at the dawn and sunrise periods. Marked "splits" are also to be noted at such times, which may be attributable to double refraction phenomena. The tendency of the effective height on 4095 kc to reach a minimum at times approximating those at which the E layer becomes "critical" for 2050 kc is also clearly marked. The rise in height from 8 A.M. to noon is clearly shown by measurements, and may be perceived visually by a close examination of the 4095 kc records. This may be a true rise in the layer or merely a change in effective height, due in part to the ionization in the E layer (2). The absence of reflections during the night on this frequency is probably due to an insufficient electron and ion concentration to refract waves of this frequency at this time. Weak reflections, however, have been observed on this frequency during the period between the characteristic post-sunset rise and sunrise fall of the layer. These reflections are, however, usually weak during the late night period, and may be due to reflection rather than true refraction phenomena (2). Usually, the reflections experience a marked discontinuity at dawn as shown on 2050 kc on the morning of February 17. The rapid rise in intensity as evidenced by the multiple reflections and photographic strength strongly suggests that true refraction may begin at this period. Similar discontinuities are frequently observable at sunset.

A more complete discussion of experimental results and their interpretation will be included in a later paper.

Ionization in the Upper Atmosphere at About 200 km Above Sea Level*

E. O. HULBURT, *Naval Research Laboratory*

(Received March 17, 1933)

From the skip distances of radio waves measured in temperate latitudes during 1927 and 1928 the average day ionization is calculated to be at about 200 km above sea level with a maximum electron density of 7.5×10^5 and 5.6×10^5 for a summer and winter day, respectively, which agree with the observed virtual heights from radio echo experiments and the longest wave which at normal incidence pierces through the ionized layer. The ratio 1.33 of summer to winter day electron density agrees with the ratio 1.42 calculated from ionization by the ultraviolet light of the sun. An average night ionization of 2.5×10^5 and 1×10^5 for summer and winter at 160 km is in rough accord with the radio facts as far as they are known, but within limits a more dense ionization at a higher level, or a less dense at a lower level, would accord equally well. The average day ionization for 1927 and 1928 is 6.5×10^5 electrons cm^{-3} which, when compared with the value 4.3×10^5 calculated from the skip distances of 1923 and 1924, shows that *the ionization increased by about 50 percent from minimum to maximum solar activity.*

I. INTRODUCTION

EXPERIMENTS with radio waves are usually interpreted as showing that there exist in the high atmosphere of the earth two prominent regions of ionization, one at about 160 to 250 km above sea level and one at about 90 to 130 km above sea level, the maximum density of the ionization in the upper region being greater than in the lower. The upper region was discovered by means of the skip distance phenomena of the short radio waves below 40 meters in length[1] and simultaneously and independently by the radio pulse experiments of Breit and Tuve[2] with 70 meter waves. The results of Breit and Tuve also gave indications of the lower region. The experiments of Appleton and Barnet[3] with 400 meter radio waves, again simultaneously and independently, demonstrated the existence of the lower region of ionization. Thus those who looked at the high atmosphere with the short waves saw only the upper region, those who looked with the long waves saw only the lower region and those who looked with waves of intermediate length saw both regions. During recent years the two regions have been investigated to some extent by means of radio wave experiments to determine the heights of the regions above sea level and the amounts of ionization in them. It is the purpose of this paper to discuss the upper region of ionization in the light of recent radio measurements such as the apparent height of the region above sea level, the skip distances of short radio waves and the penetrating wavelengths.

Although it is customary to speak of two regions of ionization and to denote the upper one by F and the lower one by E, the exact shape of the y, z curve has not yet been determined, y being the electron or ion density and z the height above sea level. All that is known is that at about 80 km above sea level y increases fairly rapidly as z increases to about 130 km, then increases less rapidly, and somewhere above 150 km y increases more rapidly again reaching a maximum value somewhere above $z=160$ km. In the following treatment it is justifiable to a first approximation to neglect the effect of the E layer on the F layer observations. We shall deal with conditions of average solar quiescence, that is, no strong magnetic storms.

II. DATA OF RADIO

From radio transmission data for the years 1927 and 1928 the skip distances of radio waves below 50 meters in length were summarized by Taylor and Young.[4] The skip distances $2s$ for a

* Published with the permission of the Navy Department.

[1] Taylor and Hulburt, Phys. Rev. **27**, 189 (1926).

[2] Breit and Tuve, Phys. Rev. **28**, 554 (1926).

[3] Appleton and Barnet, Proc. Roy. Soc. **A109**, 621 (1925).

[4] *Radio Engineering Handbook*, 1933, edited by Henny, McGraw-Hill, page 442.

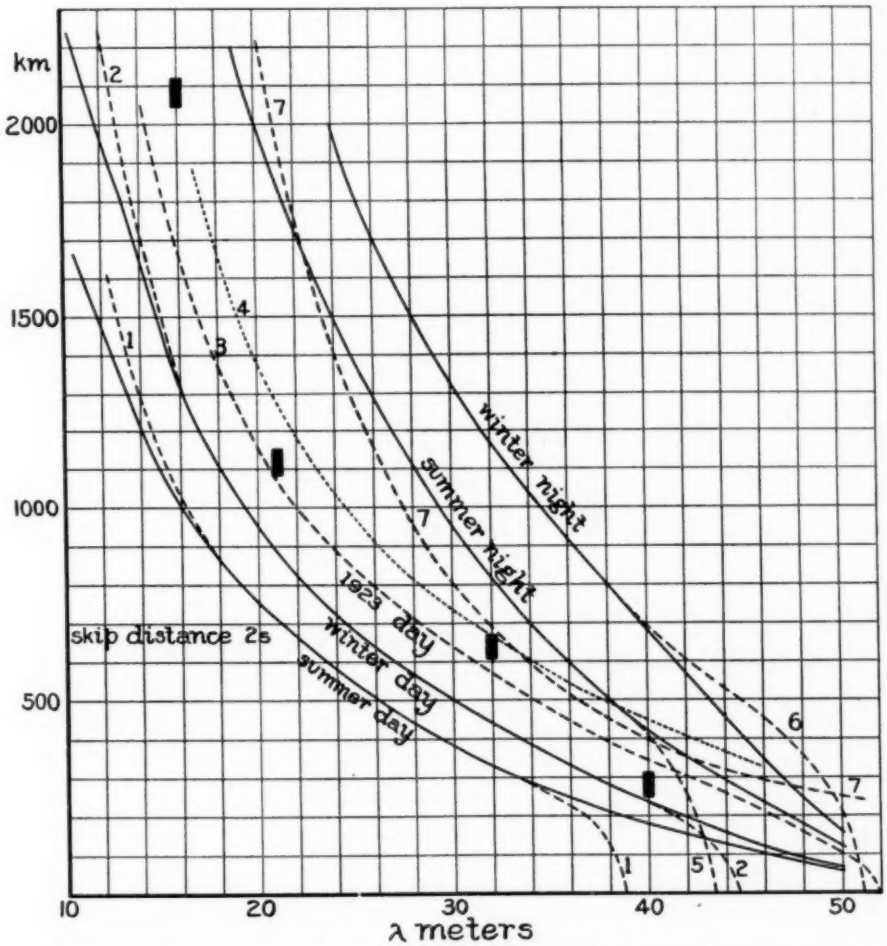

FIG. 1. Full line curves are the observed values of the skip distances for the years 1927 and 1928, the four black rectangles for 1923 and 1924, according to Taylor and Young.[1, 4] The dotted curves are theoretical.

summer and winter day and a summer and winter night in temperate latitudes are plotted as ordinates in the full line curves of Fig. 1 against the wave-length λ as abscissa. The skip distance is not a very accurate quantity, it is particularly erratic at night. The values in Fig. 1 were general averages of a large number of observations in latitudes mostly from 30° to 45°.

Investigations[5, 6, 7, 8] by the radio echo method of Breit and Tuve[2] show that the apparent or virtual height of the upper layer is around 200 to 250 km during the day and increases during the night to values often over 400 km in the small hours of the morning; it does not fluctuate very much with the season. The apparent height in the daytime is roughly constant with the wave-length of the radio pulse for waves from about 50 to over 100 meters although some of the observations show that the apparent height increases to some extent with a decrease in wave-length. At night the apparent height increases unmistakably with a decrease in wave-length, being, for example, 400 and 300 km for wave-lengths 97 and 184 meters, respectively, at 4 A.M. on April 6, 1929,[6] and 350 and 250 km for 73 and 188 meters at 11 P.M. on September 17, 1930.[7] Dr. Kenrick

[5] Tuve and Dahl, Proc. Inst. Rad. Eng. **17**, 1513 (1929).
[6] Schaffer and Goodall, Proc. Inst. Rad. Eng. **19**, 1434 (1931); **20**, 1131 (1932).
[7] Gilliland and Kenrick, Proc. Inst. Rad. Eng. **20**, 540 (1932); Gilliland, Kenrick and Norton, Proc. Inst. Rad. Eng. **20**, 286 (1932).
[8] Mitra and Rakshit, Phil. Mag. **15**, 20 (1933).

of Tufts College, Massachusetts, has kindly permitted me to reproduce three radiograms which he obtained with his apparatus for recording continuously the ionized layers.[9] These are given in Figs. 2, 3 and 4, and show very beautifully the increase in the apparent height at night, its approximate constancy with wave-length during the day and its variation with wave-length at night. The figures also yield many other facts which are not within the province of the present discussion. Actually there were moderate magnetic disturbances in progress when Figs. 2, 3 and 4 were obtained, but the figures are fairly representative of undisturbed conditions.

In the Breit and Tuve method echoes are received from overhead unless the wave-length of the transmitted pulse is too short. Let us call the wave-length which marks the transition from echoes to no echoes the "critical penetrating wave-length" and denote it by λ_p. To explain the lack of echoes for waves less than λ_p two suppositions are possible, either the waves are weakened to indistinguishability by absorption or they pierce through into space and do not return. The second supposition is usually true in the case of the short waves (it is merely a corollary of the skip distance theory[1]) and therefore λ_p is the longest wave which at normal incidence just pierces through the ionized region (it is the wave for which the skip distance is just zero). From λ_p the maximum value of the electron or ion density y may be calculated (see Eq. (3)). λ_p varies considerably with

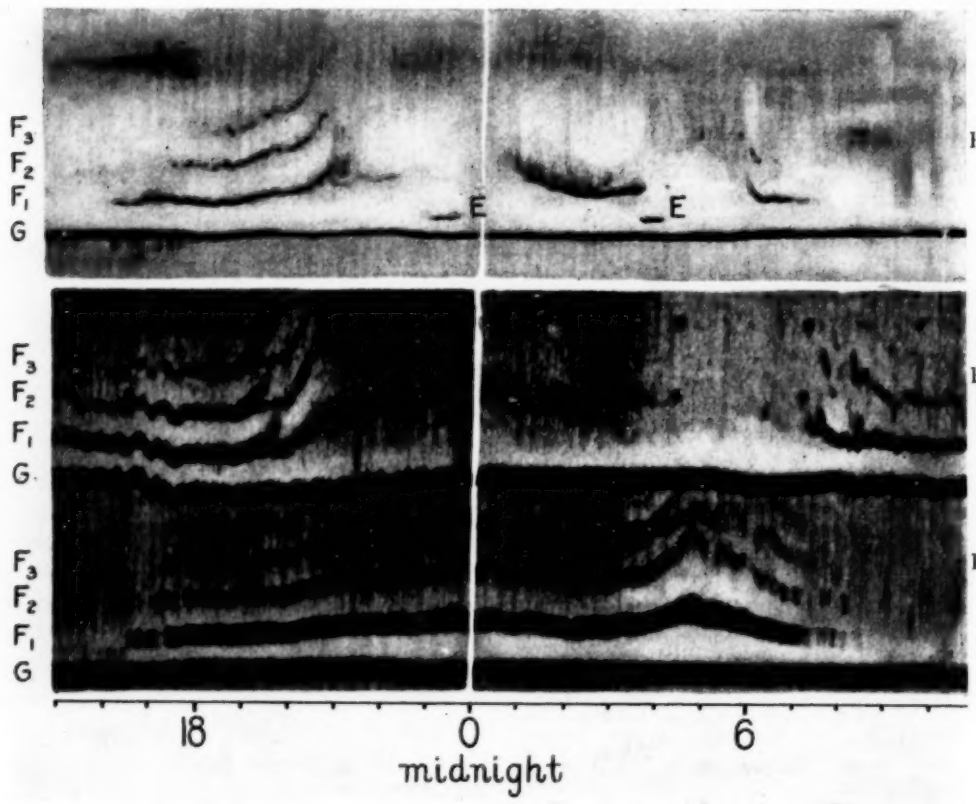

FIG. 4.

FIG. 3.

FIG. 2.

FIGS. 2, 3 AND 4. Ionized layers of the upper atmosphere recorded by Kenrick[9] at Boston, Massachusetts. G is the ground, F_1, F_2, F_3, etc., are the 1st, 2d and 3d echoes from the upper layer, E (Fig. 3) from the lower layer. Figs. 2 and 3 were obtained simultaneously with 146 and 73 meter waves on Feb. 14–15, 1933, and Fig. 4 with 125 meter waves on January 26–27, 1933. The height and time scales are linear and the same on all the figures, the apparent height being about 230 km at 3 P.M.

[9] Kenrick, Physics **4**, 194 (1933).

magnetic storms but how much is not yet known. A few observations of the diurnal and seasonal variation of λ_p are available; at night the values of λ_p are erratic, probably much as the skip distances are. During the day in the fall of 1931 in latitude 42° north λ_p was about 47 meters[6]; in India, latitude 12° south, the day value of λ_p was below 42 meters.[8] For a summer night in temperate latitudes λ_p was sometimes as large as 125 meters and sometimes below 70 meters[5, 6, 7]; for a winter night λ_p was below 146 meters (see Fig. 2). The result appears to be that in temperate latitudes an average value of λ_p is about 40 meters for a summer day, 50 meters for a winter day, and, very uncertainly, about 70 meters for a summer night and 100 to 130 meters for a winter night.

III. Average Daytime Ionization

The height h of the upper layer and the maximum density of ionization y are calculated from the skip distances by the methods of the former paper.[1] We begin by assuming that the ionization sets in sharply at a height h so that the radio waves are reflected from the lower surface of the bank of ionization as by a partially reflecting mirror; we pass later to the case of refraction. To simplify matters it is assumed that the electric vector of the radio wave is polarized in a plane parallel to the magnetic field of the earth. The results will be accurate for ions, and a fair average for electrons, for all states of polarization. The skip distance $2s$ is given by[1]

$$1-\frac{ye^2\lambda^2}{\pi m}=\frac{R^2\sin^2(s/R)}{R^2\sin^2(s/R)+[R+h-R\cos(s/R)]^2}, \quad (1)$$

where R is the radius of the earth, m is the mass of the electron or ion and e is the charge in c.g.s.e.m.u.

When the two unknown quantities h and y were adjusted so that (1) fitted the observed summer day $2s$, λ curve, h came out to be 220 km and y to be 7.5×10^5 electrons cm^{-3}; the calculated $2s$, λ curve is given by the dotted curve 1, Fig. 1. Similarly the calculated winter day $2s$, λ curve was determined and is plotted in the dotted curve 2 with $h=220$ km and $y=5.6\times10^5$ electrons cm^{-3}. It is seen that the theoretical curves agree well with the observed curves. If the ionization is made up of singly charged ions rather than electrons the values of y must be multiplied by the ratio of the mass of the ion to the mass of the electron. The height 220 km is in accord with the observed day heights from 200 to 250 km. Instead of assuming as has just been done a y, z curve such that the radio waves are reflected we may assume that the waves are refracted by an ionization in which y sets in more or less gradually with z. If the y, z curve is convex to the Z axis we obtain the same calculated curves 1 and 2 with the same maximum value of y, but with h less than 220 km, the exact value of h depending on the form of the y, z curve.[1] Therefore h is an apparent or virtual height, the true height of the day ionization bank may be 220 km or less, but is not greater than 220 km.

To find λ_p the refractive index μ is put equal to zero in the Lorentz dispersion equation

$$[a+1/(\mu^2-1)]^{-1}=-ye^2\lambda^2/\pi m, \quad (2)$$

in which the magnetic field of the earth is neglected. The quantity a, as shown by Lorentz, is 0 or 1/3, or something in between, depending on the effect of the medium on the dispersion electron. It is not certain what value of a is to be preferred, the exact value probably is a function of the nature of the collisions of the electrons, and for simplicity we put $a=0$. This gives

$$\lambda_p^2=\pi m/ye^2. \quad (3)$$

If $a=1/3$ is used all the values of y of the present paper should be multiplied by 3/2, but no other important changes occur, it being a purely formal matter to insert a factor 2/3 in (3) and to get a y greater by 3/2 than the y of (3). (3) may also be obtained by setting $s=0$ in (1). With $y=7.5\times10^5$ for a summer day λ_p from (3) was 39 meters and with $y=5.6\times10^5$ for a winter day λ_p was 44 meters, which agree with the observed values of about 40 and 50 meters.

Altogether the observed daytime skip distances, apparent heights from echo experiments and values of λ_p are fairly well accounted for

by an ionization which sets in sharply at about 220 km, or better, and what is physically more probable, by an ionization which sets in not quite so sharply with the maximum of ionization at about 200 km. This agrees with the conclusion, derived independently, that the ionization in the upper atmosphere due to the highly absorbed ultraviolet light of the sun would, because of diffusion and losses by oxygen attachment of electrons and recombination, form a bank at about 200 km.[10]

At the maximum of the y, z curve the loss of electrons due to diffusion is only about 1/3 of their loss due to attachment to oxygen molecules. Therefore very approximately the day value of y at the maximum of the y, z curve due to the ultraviolet light of the sun is given by[10]

$$by = q \cos \zeta, \tag{4}$$

where b is the attachment coefficient of electrons to oxygen molecules, ζ is the zenith angle of the sun and q is a constant; b is a function of the temperature. Taking averages over the hour of the day from an hour after sunrise to an hour before sunset and over the season for summer and winter day conditions at latitude 35°, the average temperature is 300° and 340°K, b is 9.0 and 8.3×10^{-14}, and ζ is 44° and 63°, respectively. These in (4) give 1.42 as the ratio of y in summer to y in winter for day conditions. Nearly the same ratio is obtained if instead of (4) ions and ionic recombination are assumed. The ratio given by y from the skip distances is $7.5\times10^5 \div 5.6\times10^5 = 1.33$. The agreement is about as good as might be expected from the roughness of the calculation.

IV. The Average Day Ionization for Epochs of Maximum and Minimum Solar Activity

The average value of y over the year for the years 1927 and 1928 is $(7.5+5.6)\times10^5/2 = 6.5\times10^5$. It is of interest to compare this with the value of y obtained from the day skip distances over the year for the years 1923 and 1924 given in the former paper.[1] They are shown by the black rectangles in Fig. 1. The former calculation[1] from these, with the right-handed circularly polarized wave, gave $h = 240$ km and $y = 4\times10^5$. Rather than to use these values it is better for the present purposes of comparison to recalculate the $2s, \lambda$ curve for 1923 and 1924 for the wave plane polarized with electric vector along the earth's magnetic field and with $h = 220$ km. y came out to be 4.3×10^5 and the curve is shown in curve 3, Fig. 1; it agrees passably with the four observed points.

Solar activity varies roughly in an eleven year period, minimum activity occurred in 1923 and 1924 and maximum activity around 1928. We may conclude that the maximum daytime ionization in the upper layer averaged over the year increased from about 4.3×10^5 electrons cm^{-3} for the epoch of minimum solar activity to about 6.5×10^5 electrons cm^{-3} for the epoch of maximum solar activity, an increase of about 50 percent. The observed change in the solar diurnal variation of terrestrial magnetism is about this amount, actually from 40 to 100 percent,[11] and the agreement is in keeping with the theory of the solar diurnal variation which ascribed the variation to the diamagnetism[12] of the upper atmospheric ionization.

V. Ionization at Night

Thus far the going has been smooth, but in the case of night conditions we find uncertainties. Turning to the night skip distances we first attempt to fit the observed $2s, \lambda$ curve for summer night by assuming reflection at 220 km, the day value of h. Passing the $2s, \lambda$ curve calculated from (1) through $2s = 480$ km and $\lambda = 38.5$ meters gives $y = 3.5\times10^5$ electrons cm^{-3}, or an equivalent number of ions. Curve 4, Fig. 1, is the resulting curve, it does not agree with the observed summer night curve. Redetermining the constants h and y it is found that $h = 450$ km and $y = 5.9\times10^5$ yields curve 5 which agrees well with the summer night curve. Similarly, $h = 450$ km and $y = 4.3\times10^5$ gives curve 6 which agrees with the curve for winter night. At first sight $h = 450$ km would appear to agree roughly with the observed virtual nighttime heights from the echo experiments. Such a view, however, leads

[10] Hulburt, Phys. Rev. **31**, 1018 (1928); **39**, 977 (1932).

[11] Angenheister, Handbuch der Physik **15**, 305 (1927).

[12] Gunn, Phys. Rev. **32**, 133 (1928).

to difficulties. An ionization which sets in abruptly at 450 km would give echo heights of 450 km for all wave-lengths, whereas the night echo heights are observed to increase with decrease in wave-length. Theoretical considerations[10] based on hypotheses which are acceptable at the present time, indicate very clearly that there can be no permanent or quasi-permanent banks of ionization much above 200 km. Further, with $y=5.9\times10^5$ λ_p from (3) is 43 meters and with $y=4.3\times10^5$ λ_p is 51 meters. The observed summer and winter night values of λ_p, although not accurately determined, are much greater, being around 70 and 100 to 130 meters, respectively, which require y to be about 2.5×10^5 and 1×10^5 electrons cm^{-3} or an equivalent number of ions. The conclusion is that an ionization bank at 450 km is not in agreement with observation, we must have a less dense ionization at a lower level with a y, z distribution curve such as to give agreement with the skip distances and the echo heights.

In illustration, let us assume that there are no electrons from sea level to a height h_o, and that from h_o to h'

$$y=\beta z^{\frac{1}{2}}, \qquad (5)$$

where β is a constant. This is Case 4a, reference 1. Above h' (5) ceases to hold, y above h' decreasing, so that y is a maximum at $z=h_o+h'$. From the skip distance formula, Eq. (30), reference 1, for a flat earth the *2s*, λ curve was determined with $h_o=160$ km, $h'=2$ km and with 3×10^5 for the maximum value of y. The curve was transformed to a curved earth and is plotted in the dotted curve 7, Fig. 1. It agrees fairly well with the observed summer night *2s*, λ curve. With $y=3\times10^5$, λ_p is 61 meters which is not far from the observed value about 70 meters. The calculated apparent heights for 80 to 100 meter waves at normal incidence increase as the wave-length is decreased, but are below the observed values, being less than 200 km. Therefore the distribution (5) does not give exact agreement with all the facts. The calculation is of value, however, in that it indicates that it is possible, although mathematical difficulties may be troublesome, to find an ionization with a maximum value of y about 2 or 3×10^5 at a height below 200 km and with a y, z distribution curve of the proper sort to account for all the nighttime skip distances and virtual heights. To attempt to do this in further detail now seems premature; it is better to wait until the experimental data for night conditions are more clearly determined.

If the foregoing discussion is correct it follows that the daytime virtual heights from the echo experiments are pretty close to the true height of the upper layer of ionization and that the night virtual heights are not close at all but are much greater than the true height. As a theorist I find no objection to this conclusion, but as an experimenter when I look at curves such as those of Figs. 2, 3 and 4, I wonder if the theorist is correct. Thus we close with a note of uncertainty which only future experiment can dispel.